Journal of
Composites Science

Article

Studies on the Mechanical, Strengthening Mechanisms and Tribological Characteristics of AA7150-Al_2O_3 Nano-Metal Matrix Composites

K. Chinna Maddaiah [1,2], G. B. Veeresh Kumar [2,*] and R. Pramod [3]

1 Mechanical Engineering Department, Chamakura Malla Reddy (CMR) Engineering College, Medchal Road, Hyderabad 501401, Telangana, India; chinnasiri0424@gmail.com
2 Mechanical Engineering Department, National Institute of Technology-Andhra Pradesh, Tadepalligudem 534101, Andhra Pradesh, India
3 Mechanical Engineering Department, Amrita School of Engineering, Amrita Vishwa Vidyapeetham, Bengaluru 560035, Karnataka, India; r_pramod@blr.amrita.edu
* Correspondence: veereshkumargb@nitandhra.ac.in; Tel.: +91-9972455343

Abstract: Stir-casting with ultrasonic cavitation produced nano-Al_2O_3-filled AA7150 matrix composites in this study. The SEM microstructure study shows that all composites include nano-Al_2O_3 particles with consistent particle sizes and homogenous distribution. EDS and XRD showed no secondary phases or impurities in the composite. Optical microscopy showed intense ultrasonic cavitation effects, and nano-Al_2O_3 particles caused grain refinement in the AA7150 matrix. The composite's mechanical characteristics improved when the Al_2O_3 nanoparticle weight percentage (wt.%) increased. With only 2.0 wt.% nano-Al_2O_3 particles, the composites yielded 232 MPa, 97.52% higher than the sonicated AA7150 matrix alloy. Multiple models were used to characterize the strength of the AA7150 nano-Al_2O_3 composite. The findings showed that thermal incongruity, Orowan strengthening, the Hall–Petch mechanism, and load transfer effects contributed the most towards the increased strength of the composite. Increasing the nano-Al_2O_3 wt.% in the AA7150 matrix improved hardness by 95.08%, yield strength by 90.34%, and sliding wear resistance by 46.52%. This enhancement may be attributed to the combined effects of better grain refinement, enhanced dispersion with dislocation strengthening, and better load transfer between the matrix and reinforcement, which are assisted by the inclusion of reinforcements. This result was confirmed by optical studies.

Keywords: AA7150-Al_2O_3 composites; ultrasonic cavitation; mechanical properties; dislocation; wear; strengthening mechanism

check for updates

Citation: Maddaiah, K.C.; Kumar, G.B.V.; Pramod, R. Studies on the Mechanical, Strengthening Mechanisms and Tribological Characteristics of AA7150-Al_2O_3 Nano-Metal Matrix Composites. *J. Compos. Sci.* **2024**, *8*, 97. https://doi.org/10.3390/jcs8030097

Academic Editors: Francesco Tornabene, Salvatore Brischetto and Thanasis Triantafillou

Received: 20 November 2023
Revised: 13 January 2024
Accepted: 21 February 2024
Published: 7 March 2024

1. Introduction

Aluminum alloy (AA) nanocomposites are widely utilized in various engineering sectors for their exceptional attributes, including mechanical strength, resistance to corrosion, and an impressive strength-to-weight ratio. These materials are pivotal in structural usage within aerospace and automobile manufacturing to address ever increasing demands from the inductrial sector, mainly with respect to enhanced performance and properties in comparision to conventional materials [1,2]. The 7XXX series alloys are well-regarded within these applications for their lightweight nature, higher toughness, ultimate tensile strength (UTS), fatigue, and fracture resistance, making them crucial components in aviation, air transportation, and space-related applications [3]. Integrating composite materials reinforced with hard phase particles has paved the way for improved wear resistance and strength [4]. Research into aluminum (Al) metal matrix composites (MMCs) filled with TiC nanoparticulates with a lower coefficient of thermal expansion (CTE), higher melting point, hardness, and resistance against wear has gained recent popularity [5]. It was concluded that the micro-hardness of the coated layer is increased due to the formation of metallic carbides on the surface of the samples during the electric discharge coating [6]. The different range of surface fouling methods, physical surface, micro and nano-size surface texture production methods were discussed in detail in a study by Abhijit Cholka et al. [7]. It was observed that the smooth and hard surface provided fatigue and wear resistance.

In micro to nano-sized particles, smaller particle dimensions enhance mechanical properties but tend to result in larger clusters and agglomerates [8]. A primary obstacle is attaining the required characteristics in liquid metals by distributing nanoscale reinforcing particles uniformly [9]. For this reason, the two-stage stir-casting method is favoured, as it offers maximal yield with minimal investment, reduced waste, and minimal damage [10]. The improved fatigue and high-temperature creep resistance of several alloys have been shown in numerous investigations [11]. However, creating Al-MMCs with ultrafine nanometer (nm) particles in liquid metal is complex, resulting in poorly wettable agglomerates that impede uniformity. For dispersing ultrafine particles in melts of Al-based alloys, a two-step stir-casting technique has shown to be a good option in this context [12]. Because liquid casting is flexible and affordable, it is highly advised for Al-based MMC production [13].

Recent studies show that metal matrix nanoparticle-reinforced composites (MMNCs) have improved mechanical and tribological characteristics than MMCs with micron-sized reinforcement additives. A 50% increase in yield strength (YS) with just 2.0 wt.% SiC nanoparticles added to A356 alloy [14] demonstrates excellent ductility, resistance against fatigue, and creep-related properties maintained even with small amounts of nano-scaled particles. Similarly, adding 2.0 wt.% nano-SiCp to A356 alloy MMCs resulted in a 22% rise in tensile strength [15]. The particulate reinforcement inside the base matrix alloy has been shown to increase the aging process of Al alloys. This enhancement occurs due to the accumulation of dislocations near the strengthening mediums, as demonstrated by previous studies. Despite the significant enhancement in the mechanical behaviour of MMCs owing to the incorporation of ceramic particulates, the introduction of reinforcement beyond a certain volume percentage ultimately induces micro-cracks and reduces structural integrity [16].

Despite the notable benefits of MMNCs, the current industry manufacturing methods could be more cost-effective and reliable for producing bulk composites with intricate component configurations. Commonly used methods include powder metallurgy and stir-casting with ultrasonic cavitation [17]. Among these approaches, stir-casting has acquired attention as an economical, straightforward, and efficient method for creating near-net-shaped components from bulk-size composites [18].

Nevertheless, a significant challenge in preparing MNCs via stir-casting lies in the need to achieve a consistent and even distribution of nanoparticles. This effect can be primarily explained by the considerable variation in the density between the matrix and nanosized particulates, and the notably higher specific surface area of the nanosized reinforcing particulates. As a result, there is insufficient wettability between the matrix alloy and nanosized particulate reinforcement [19]. Therefore, a considerable number of researchers have adopted the use of stir-casting in conjunction with the ultrasonic cavitation approach. In this methodology, nanoscale reinforcements are mechanically dispersed in a molten alloy matrix through stirring. Subsequently, the resulting liquid slurry of matrix reinforcement undergoes ultrasonic treatment to disintegrate clusters and agglomerations of reinforcement particles, thereby ensuring their homogeneous dispersion. This dispersion is achieved before transferring the slurry into the casting die for the subsequent solidification process. With reference to the above, there is a lack of information available in the literature about the characterization of the nano-sized Al_2O_3 pariculate reinforced AA7150 composites with regards to the strengthening mechanisms and wear performance. The present study included the preparation of AA7150-Al_2O_3 np composites utilizing a stir-casting method aided with an ultrasonic cavitation technique and its effects on the physical, mechanical, and tribological characteristics of the composites fabricated. The study also discusses the strengthening mechanisms under nanoparticle reinforcements and improvisations observed in strength, hardness, grain refinement, and resistance against wear. This present study will also aid in utilizing the fabricated composites in the aeronautical and automobile industries.

2. Materials and Methods

The authors employed a commercially available AA7150 alloy sourced from Vision Castings and Alloys, Telangana, India, as the base alloy in this investigation. This alloy is well-known for its outstanding strength and is extensively used in fabricating diverse structural components for aerospace and locomotive applications [20]. Examples of such automotive parts include rocker arms, brake callipers, pistons, and wheels [21].

The selected Al matrix and reinforcing nano Al_2O_3 particles, with specifications as shown in Table 1, were procured from Sigma Aldrich and have comparable densities. Their CTE, however, differs significantly. The risk of nanoparticle dispersion throughout the processing phases is reduced by this disparity [22].

Table 1. Specifications of Al_2O_3 reinforcement particles employed.

Average Size	Purity Level	C	SiO	Fe	Ni	Ca
<20 nm	>99.5%	0.059%	0.1	0.065%	0.13%	0.047%

Creating these composites involved incorporating ceramic particles into the molten alloy matrix by mechanical stirring using a steel impeller, followed by solidification. It is crucial for the reinforcement particles to wet and chemically interact with the molten matrix to ensure proper dispersion. Lower processing temperatures result in suboptimal wetting of Al_2O_3 particles in the Al melt, leading to weaker bonding between the matrix and the reinforcement [23]. Conversely, higher processing temperatures can cause the rapid development of brittle compounds due to the reaction with alloy matrix and nano Al_2O_3, potentially compromising the composite's mechanical and corrosion resistance properties. Excessive turbulence, caused by higher stirring speeds, can introduce unwanted gas entrapment, increasing porosity in the composite [24].

It is only when the molten matrix alloy thoroughly wets the surface of the reinforcement particulates that a strong binding is attained between the alloy matrix and nanoparticulate reinforcement. Hence, the temperature and stirring speed of the composite slurry were carefully regulated during preparation. The AA7150 alloy was placed within a graphite crucible diameter of 150 mm and height of 150 mm to make the blended slurry. It was heated to a temperature somewhat higher than the matrix alloy liquidus (750 °C) temperature. The electric furnace temperature was maintained at that level for twenty minutes to aid in degassing. Preheated nano-Al_2O_3 particles were added at 200 °C while the melt was agitated at 250 rpm using a steel impeller. An environment of pure argon gas was used for the motorized stirring and the insertion of reinforcement particles. A mechanical stirrer was utilized to prepare the molten composite.

The matrix-reinforcement molten composite was agitated before holding the molten composite temperature at 750 °C for five minutes. After that, a titanium sonic probe was dipped into the melted material and exposed to ultrasonic wave treatment for five minutes. The initial purpose of this ultrasonic treatment was to disintegrate larger clusters. An additional 5 minutes treatment ensured the elimination of any remaining smaller agglomerations, degassing, and refinement of the matrix grain size, as referenced in the literature [25–27]. The ultrasonic waveguide was connected to an ultrasonic converter with 1 kW power output and 20 kHz resonant frequency, utilized to produce the ultrasonic vibrations. The ultrasonic treatment procedure for the molten MMC was achieved in an inert Argon gas atmosphere. Then, the liquid composite melt was meticulously transferred into a steel mould with dimensions of 160 × 160 × 10 mm, facilitating the subsequent solidification process.

3. Results and Discussion

The X-ray diffraction (XRD) intensity peaks in Figure 1a,b clearly show that essential elements like Al, Mg, Zn, and Cu are present, along with compounds like Cu_2Mg_1, Mg_1Zn_2, and Al_2O_3. The distinguishable peaks in the XRD pictures provide a visual depiction that clarifies the chemical composition of AA7150 and the Al_2O_3 nanoparticulate MMCs.

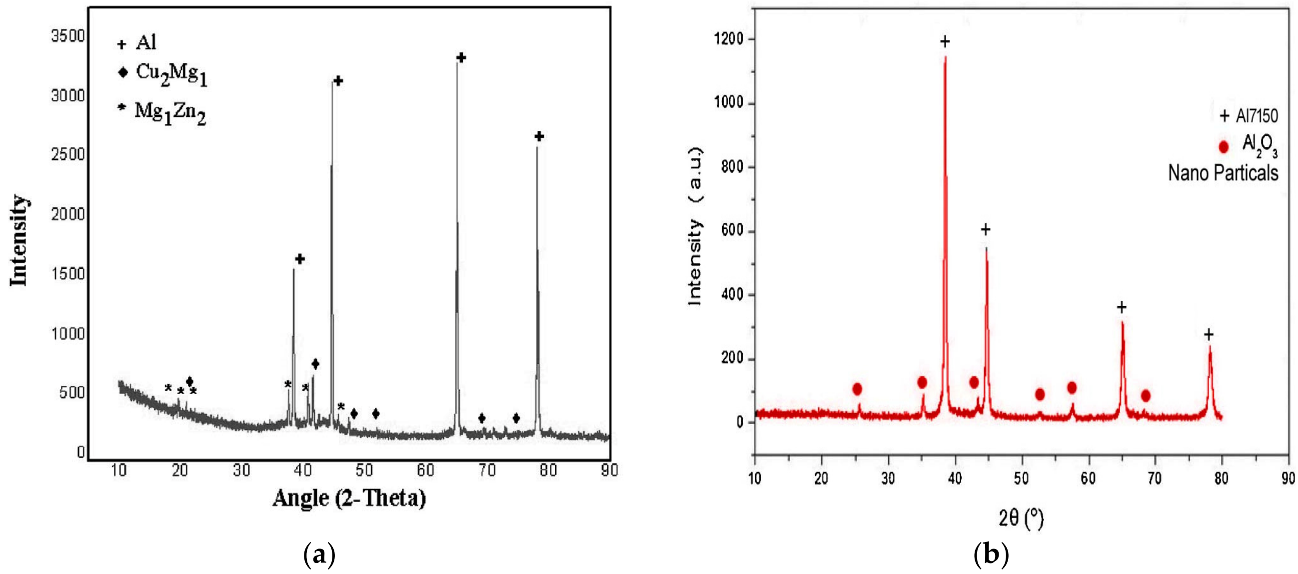

Figure 1. XRD pattern of: (**a**) AA7150; and (**b**) AA7150-Al_2O_3 nanoparticulates.

3.1. Microstructural Examination

AA7150 and AA7150-Al_2O_3 nano-composites samples of 10 × 10 × 10 mm were subjected to microscopic inspection. Assessing the material's homogeneous dispersion of Al_2O_3 nanoparticles was the primary goal. The analysis of micrographs showed that the AA7150 grains were refined with ultrasonic treatment and the inclusion of nanosized Al_2O_3 particles.

The dispersion of the reinforcement particulates inside the matrix was comprehensively investigated using high-resolution electron optical microscopy as per ASTM-E3 standards.

Figures 2a–d and 3a–d demonstrate the nanocomposite samples' optical and SEM microstructure images, showcasing the variations in weight percentages of Al_2O_3 nanoparticles inside the matrix. The SEM images reveal a scarcity of microclusters, while the nanoparticles exhibit a homogeneous dispersion inside the AA7075 matrix. This finding emphasizes the effectiveness of high-intensity ultrasonic vibrations, which may disperse particles and tear up agglomerates, producing a powerful and explosive impact through transitory cavitation.

3.2. UTS of AA7150–Al_2O_3 Nano MMCs

The ultimate tensile strength (UTS) testing adhered to ASTM E8M standards for sample preparation and testing. These samples were created using the as-cast composites as source material. A programmed universal testing machine, the FIE UTE100 type, was used for the testing, which was done at ambient temperature and with a fixed extension speed of 1 mm/min. As noticed in Figure 4a,b, compared to AA7150 alloy, the composites exhibited greater UTS, YS, and toughness under all specified reinforcement conditions. Notably, the composites still retained a high level of ductility. One noteworthy factor contributing to the enhanced mechanical behavior of the MMNCs was the incorporation of nanosized Al_2O_3 particulate reinforcement. The YS increased by 97.54% compared to the alloy matrix when adding 2.0 wt.% of nano-Al_2O_3 particles.

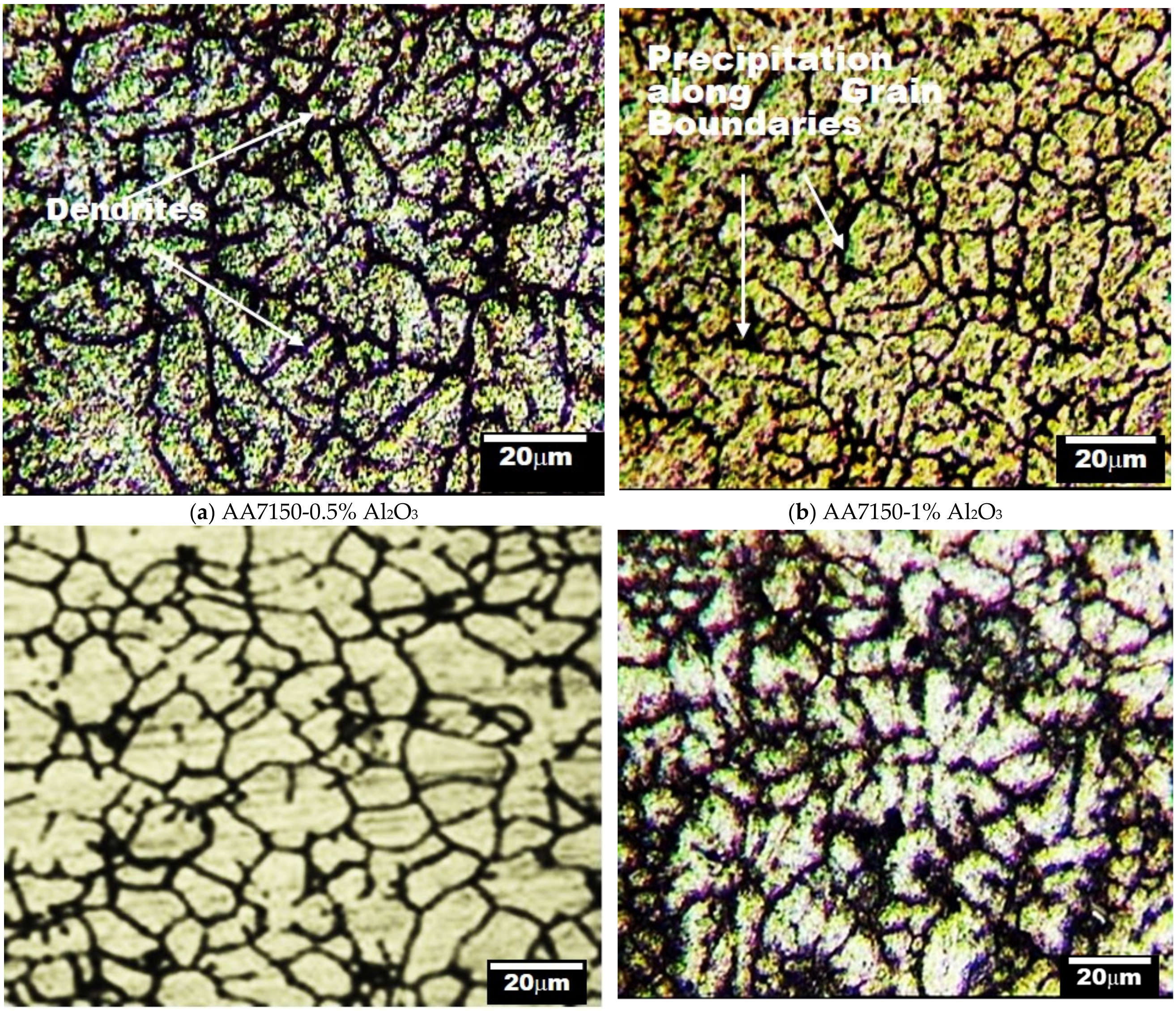

(**a**) AA7150-0.5% Al_2O_3 (**b**) AA7150-1% Al_2O_3

(**c**) AA7150-1.5% Al_2O_3 (**d**) AA7150-2% Al_2O_3

Figure 2. Optical microscope images of MMNCs fabricated in the current study.

Additionally, as the wt.% of Al_2O_3 nano reinforcement varied, the nano-MMCs strength displayed a consistent upward trend. The composite may explain this tendency, including more nanoparticle micro clusters, especially in Figure 2. There were more fracture initiation sites at the particulate–matrix interface in the 2.0 wt.% Al_2O_3 reinforced sample due to the higher density of these nanoparticle micro clusters than in the 1.5 wt.% Al_2O_3 reinforced sample. Ultimately, this caused the composite to fail prematurely [28].

3.3. Density and Micro Hardness of AA7150–Al_2O_3 Nano MMCs

For different AA7075-Al_2O_3 MMNCs compositions, theoretical density values were computed utilizing the rule of mixtures equations. The obtained values were then compared with the experimentally obtained values of density. Figure 5a visually represents the density values obtained theoretically and practically. The calculated density values are greater than the weight-to-volume density values, as seen in Figure 5a. Minor casting flaws cause this variation in the density of MMNCs, and the probability of generating processing-induced voids increases as the wt.% of reinforcement particles increases, resulting in a reduction in YS [29]. Therefore, it is essential to consider the impact of porosity to more accurately forecast the YS of MMNCs. Based on the earlier publications, porosity is the degradation factor linked to the existence of porosity in MMNCs, as represented by Equation (1), where Pd, l, and P represent particle size, particle length, and porosity volume fraction, respectively [30].

$$f_{porosity} = 1 - e^{-\left(\frac{0.405l}{P_d} + \frac{0.318P_d}{l} + 1.22\right)P} \quad (1)$$

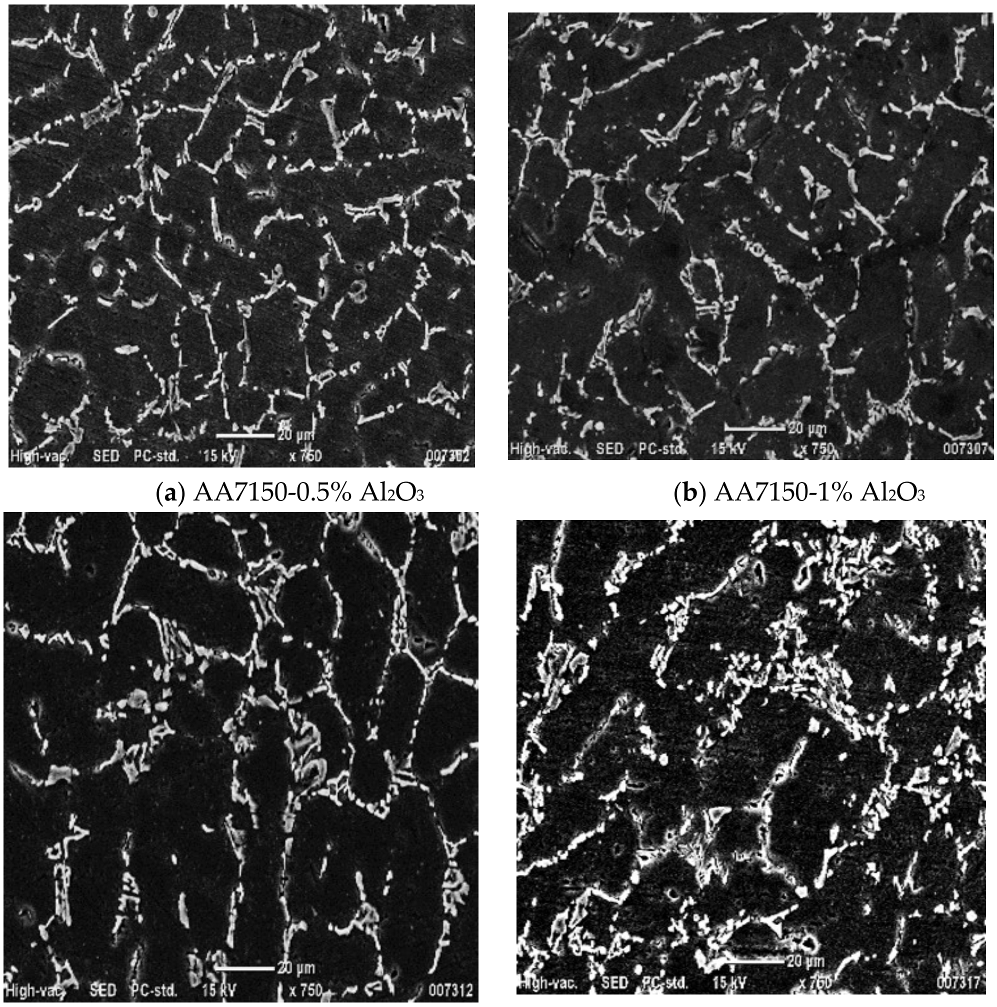

(**a**) AA7150-0.5% Al_2O_3 (**b**) AA7150-1% Al_2O_3

(**c**) AA7150-1.5% Al_2O_3 (**d**) AA7150-2% Al_2O_3

Figure 3. SEM images of MMNCs fabricated in the current study.

However, it is interesting to note that for every set of experiments, the density values rose in proportion to the amount of reinforcements in the AA7150 alloy. The addition of higher-density nano Al_2O_3 particles is what caused the density values to increase. Air entrapment after preliminary mixing, shrinkage during solidification, the development of H_2 gas, and the introduction of air in the melt or an air envelope around packed nano Alumina particle reinforcements are all responsible for the differences in porosity values of MMNCs [31].

It has been shown that the porosity of nanocomposites exhibits minimal variation as the weight percentages of nanoparticulate reinforcements rise, as shown in Figure 5b. The enhanced wetting of the molten AA7150 alloy is attributed to the influence of ultrasonic vibrations. The Al_2O_3 nanoparticles exhibit nucleation behavior, leading to grain refinement in the AA7150 matrix material. The minimal variation in the porosity percentage is due to the strong ultrasonic degassing effect on AA7150, and the consistent distribution of nanoparticles in the AA7150 liquid metal enhances its fluidity.

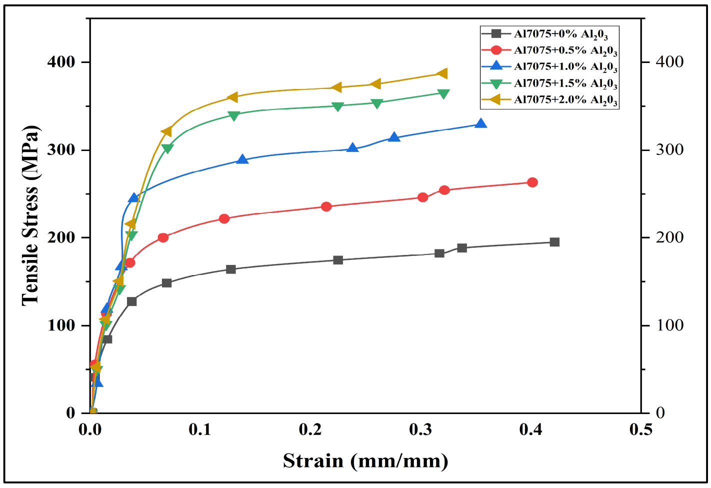

(**a**)

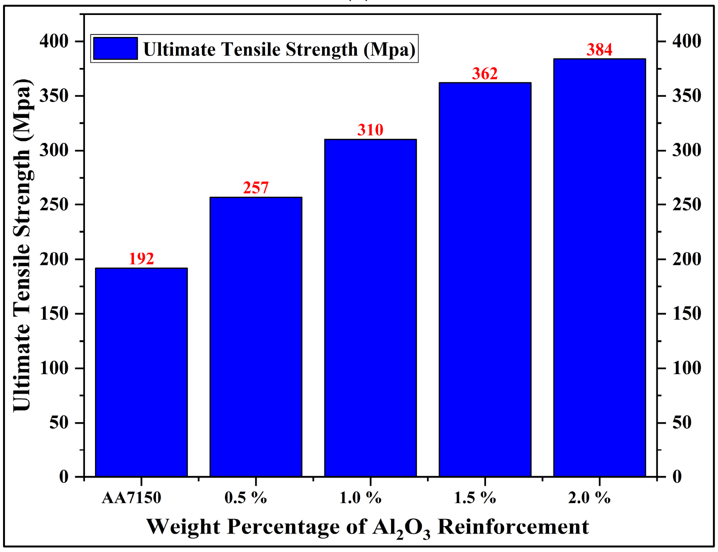

(**b**)

Figure 4. (**a**) Stress–strain curve; and (**b**) UTS of AA7150–Al_2O_3 nano MMCs.

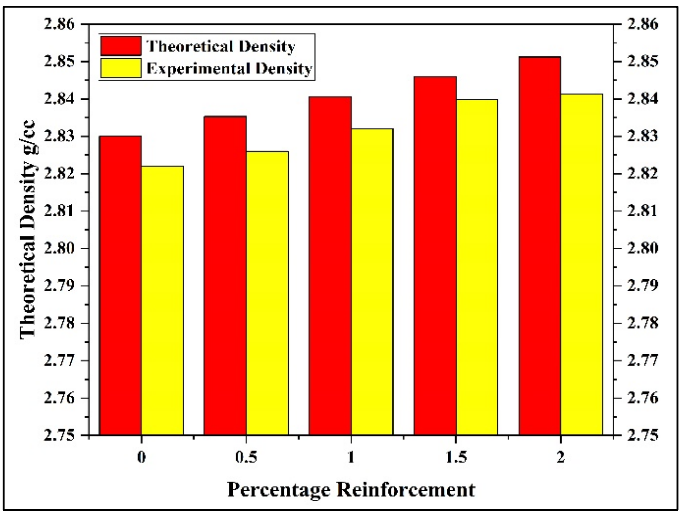

(**a**) Comparison of Theoretical vs. Experimental density of the AA7150-Al_2O_3 MMNCs.

Figure 5. *Cont.*

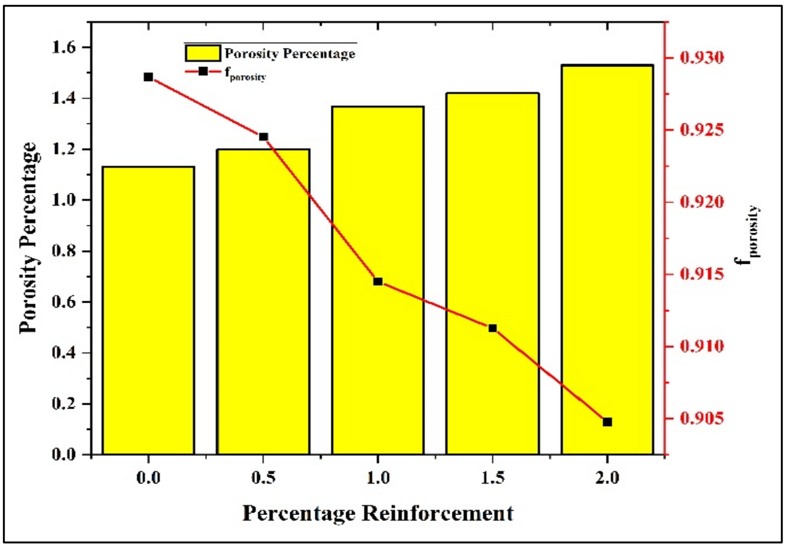

(**b**) Porosity percentage of the AA7150-Al_2O_3 MMNCs.

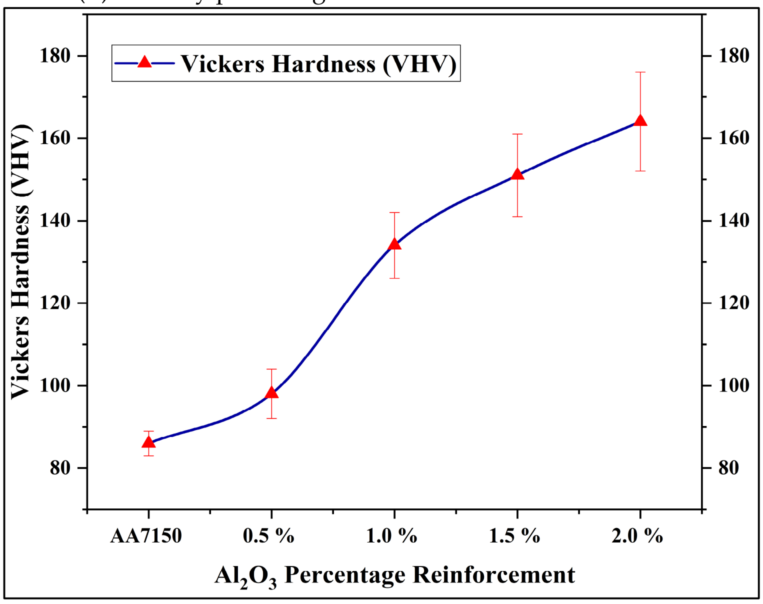

(**c**) Vickers hardness of the AA7150-Al_2O_3 MMNCs.

Figure 5. Variation of physical properties of AA7150–Al_2O_3 MMCs against wt.% of Al_2O_3.

Consequently, porosity was consistent with the stated values as the wt.% of reinforcements increased. The matrix and AA7150- Al_2O_3 MMNCs hardness were determined using Vicker's micro-hardness tester model, ECONOMET VH 1MD. The experiments were executed at ambient temperature, with a 200 g load and dwell time of 15 s, in accordance with the requirements provided in the ASTM E92 standards. This section discusses the hardness test results for the AA7150 alloy and AA7150-Al_2O_3 MMNCs. Figure 5c shows the average hardness values of the samples. Each measurement of hardness is the average of five measurements. The hardness of the MMNCs increases significantly as the Al_2O_3 concentration of the matrix alloy rises, as seen in the chart. The MMNCs with 2.0 wt.% Al_2O_3 reinforcing material showed the highest micro-hardness of all the compositions evaluated in this investigation [32].

3.4. AA7150–Al_2O_3 Nanocomposites Ductility

The properties of the composite material exhibit notable enhancements with increasing levels of reinforcement. However, when the quantity of reinforcement is raised from 0% to 2%, as noticed in Figure 6, there is a decrement in the percentage elongation of MMNCs.

The observed loss in ductility may be credited to the concurrent increase in the MMNC's hardness. The outcome indicates decreased MMNC percentage elongation when the nano reinforcement content is raised from 0% to 2%. A significant negative correlation exists between higher reinforcement content and a 6.6% reduction in percentage elongation. Nanosized Al_2O_3 particulates disperse more evenly in the base alloy matrix than in the coarser reinforcements. Thus, the MMCs reinforced with nano particulates gain enhanced strength compared to their coarse particulates reinforced MMCs. Better homogeneity is obtained as the particulate dimensions decrease from coarser to nano-size. The findings presented in this study align with the results reported in several previous studies [33,34].

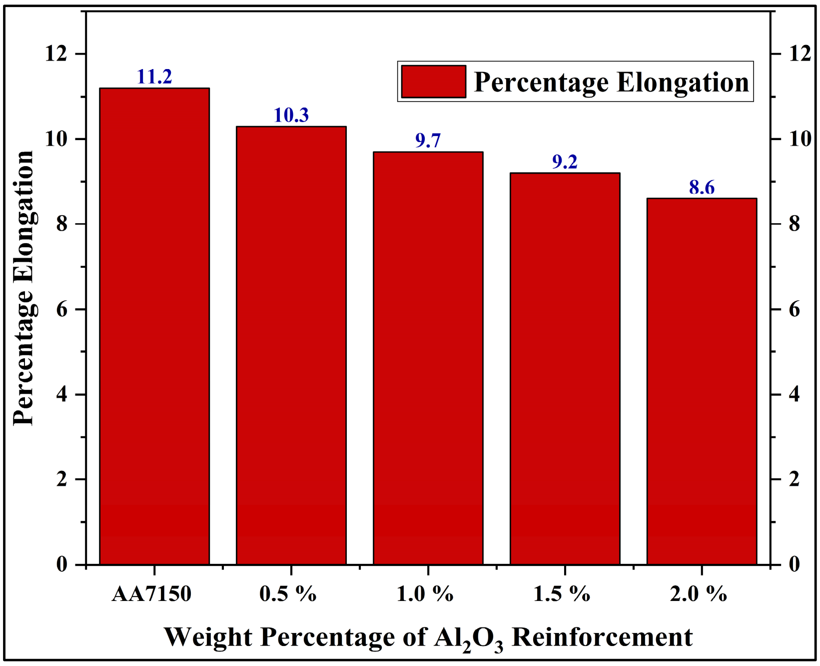

Figure 6. AA7150–Al_2O_3 MMCs' percentage elongation.

4. Strengthening Mechanisms

The influence of particulate quantity and size on the resulting composite strength is generally recognized. According to the dispersion enhancement process, it has been shown that bigger particles tend to generate voids in their vicinity, resulting in a reduction in the overall strength of the mixture [35]. A decrease in the size of the reinforcement particulates leads to decreased inter-particulate spacing inside the MMCs. Consequently, this phenomenon improves dislocation movement resistance and reinforces the overall strength of the MMCs [36]. Furthermore, incorporating nanometer-sized reinforcement particles has been shown to enhance particle hardening processes, increasing the mechanical behaviour of the matrix [37].

Diminishing the size of reinforcement particulates inside the alloy matrix mitigates the concentration of stresses at the corners of these particles. The interaction between the reinforcing particles and deflections is enhanced, leading to an overall enhancement in the strength of the MMCs [38]. The addition of ceramic nanoparticulates smaller than 100 nm has been shown to significantly enhance the composite's strength while maintaining its ductility, as revealed by research [39,40]. The addition of sufficiently tiny grains as reinforcement effectively fixes the grain borders inside the matrix, leading to a more refined grain structure [41] and heightened limitations on the movement of grain boundaries [42]. The enhanced durability of the composites may be credited to their smaller grain structure and restricted dislocation movement.

However, the Orowan reinforcement effect significantly increases when examining reinforced nanoparticles with a size below the critical value. Conversely, there is a decrease in this impact when the size of the nanoparticles exceeds the threshold mentioned above. The critical value of nanoparticle size exhibits variability, with sizes of 2 nm to 100 nm [43]. In contrast, when the particle size was reduced to 20 nm, a significant durability improvement was seen while maintaining its intrinsic flexibility. In addition, it has been shown that decreasing the dimensions of the reinforcing particles significantly improves interfacial contact. However, this decrease also reduces the load-carrying ability of the reinforcing particulates and the alloy matrix [44]. Research done by S Jayalakshmi et al. [45] showed a notable improvement in the mechanical durability of a solid Al alloy framework by integrating micrometer-sized particles.

Nevertheless, the enhancement in strength was concomitant with a decrease in ductility. The present work integrates principles from continuum mechanics and micromechanical reinforcement to explore the effect of different reinforcement processes on the composite's YS enhancement upon adding the nano-Al_2O_3 particulates. The study further analyzes the effects of varying the reinforcement ratio in the AA7150 alloy matrix on the contributions made by different reinforcing processes. Within continuum mechanics, the process of strengthening is characterized by the load transfer from a yielding matrix to inflexible ceramic reinforcing particulates. This transfer occurs as a result of the robust bonding that takes place between the particulates and the alloy matrix. Concurrently, the incorporation of hardened ceramic reinforcing particles inside the base alloy significantly impacts the foundational mechanism accountable for enhancing the strength of the composite.

4.1. Strengthening Owing to Load-Transfer Mechanism

According to continuum mechanics, the composite yield strength (σ_{yc}) enhancement results from the effective load transfer between the flexible matrix and the tough reinforcement particulates. This improvement is approximated by utilizing the following formula [46,47]:

$$\sigma_{yc} = \sigma_{ym}\left[V_r\left(\frac{S+2}{2}\right) + V_m\right] \tag{2}$$

where σ_{ym}—matrix yield strength, V_r—reinforcement volume fraction, V_m—matrix volume fraction, and S—reinforcement particulates aspect ratio, with S = 1 for particulates with a spherical or equiaxed shape.

4.2. Orowan Strengthening Mechanism

In the MMCs depicted below, the applied load leads to the initiation of fractures inside the particle agglomerates. The composites experience a gradual propagation of defects due to the consistent load application, resulting in premature failure. The use of uniform reinforcing particle dispersion, achieved via acoustic ultrasonic cavitation and streaming, leads to a notable decrease in fracture initiation within the composite material in places where particulate agglomeration occurs. The increase in YS witnessed in the Orowan strengthening may be credited to the interaction between dislocations in the alloy matrix grains and strong reinforcement particulates. This interaction prevents fracture development under applied stress. The substantial variation in the modulus of elasticity between the reinforcement particulates and the alloy matrix leads to a different interaction between reinforcement particulates and dislocations. Instead of initially being reduced through them, the dislocations undergo bowing and recoupling, eventually forming a loop surrounding the particulates. The dislocation loops, associated with Orowan strengthening, serve as barriers to the movement of dislocations, enhancing the composite's overall strength. The resistance to dislocation motion and fracture propagation will be enhanced as the percentage of reinforcement in the alloy matrix increases, thus leading to an increase in the strength of MMCs at higher reinforcement levels. Estimating the Orowan strengthening contribution to the yield power improvement in the MMCs can be found in the range of [48,49]:

$$\Delta\sigma_{Orowan} = \frac{0.13Gb}{\lambda} ln \frac{D}{2b} \tag{3}$$

The Al7075 alloy has a shear modulus (G) of 24.4 GPa, while its 'b' measures 0.286. The value of λ was determined for several scenarios, encompassing nano-Al_2O_3 reinforcement particles at concentrations of 0.5%, 1.0%, 1.5%, and 2.0%, with an average particle size (D) of 20 nm. Upon substituting these values into Equations (2) and (3), it was determined that the composite yield strength experiences an increase attributable to Orowan strengthening. Specifically, the computed increments amount to 9.8 MPa, 14.1 MPa, 20.1 MPa, and 26.7 MPa for reinforcement concentrations of 0.5 to 2.0% of nano-Al_2O_3 particulates, respectively [50].

$$\lambda = D\sqrt{\left[\frac{\pi}{6V_r} - \frac{2}{3}\right]} \tag{4}$$

'G'—shear modulus of AA7150, 'b'—Burgers vector. 'D'—average particle diameter, and 'λ'—interparticle distance, which is the distance between the edges of the particles as indicated in Equation (4).

4.3. Dislocation Strengthening Mechanism

The improved mechanical characteristics seen in MMNCs can be attributed to the greater interfacial area among the nano-Al_2O_3 and AA7150, which results from the incorporating nanosized particles. Furthermore, the thermal mismatch between nano-Al_2O_3 particulates and the AA7150 matrix induces thermal stresses upon cooling from the processing temperature. These stresses, enough to cause plastic deformation, primarily occur in the interfacial region due to the thermal equilibrium established merely at the contact temperature during the process. The aforementioned stresses rapidly decrease as the distance from the boundary increases. Consequently, this phenomenon may lead to minute imperfections, such as dislocations, in the immediate proximity of particles of nanoscale dimensions. Experimental observations have confirmed the existence of dislocation density close to the interface separating the matrix and reinforcement. The high atomic-level cohesion between the matrix and reinforcement is due to the nanoparticles and the technologies used for sound synthesis. This cohesion is characterized by direct bonding between the nanoparticles and the matrix.

The MMNCs' YS is often defined as the stress needed to initiate dislocation sources. This property is guided by the existence and size of several impediments that impede the dislocations' movement within the alloy matrix.

The volumetric strain within the solidified composite arises from the considerable difference in the CTE between the nano-Al_2O_3 reinforcement and alloy matrix, in line with the Taylor strengthening process. The presence of this particular strain induces the generation of geometrically necessary dislocation (GND) loops in the vicinity of the reinforced particles. These GNDs counterbalance the dislocations that arise owing to the significant variation in the CTE. As a result, the composite yield strength is enhanced. The MMCs' strength increases as the number of particulates inside it increases, resulting in a higher occurrence of GND loops. The composite yield strength augmentation by dislocation strengthening may be evaluated using Equation (5), as proposed by the Taylor strengthening mechanism [51,52]:

$$\Delta\sigma_{CTE} = \eta Gb\sqrt{\rho} \tag{5}$$

In the present context, the symbol "η" represents a value roughly equal to 1 [53]. The alloy matrix's shear modulus (G) has a specific value of 26 GPa. On the other hand, the symbol "b" represents the Burgers vector, which is measured to be 0.286 nm, as stated in references [54]. Furthermore, the dislocation density (ρ) results from the CTE mismatch, and fd is the improvement factor based on the dislocation density. These are approximated using Equations (6) and (7), respectively:

$$\rho = \frac{12\Delta\alpha\Delta T V_r}{DbV_m} \tag{6}$$

$$f_d = kGb\sqrt{\rho}/\sigma_{ym} \tag{7}$$

Within this framework, the symbol Δα denotes the inconsistency in the CTE between the reinforcement particulates, which have a value of 4.6 × 10^{-6} K^{-1}, and the alloy matrix, which has 760 °C of 23.6 × 10^{-6} K^{-1}. The temperature variance (ΔT) between the initial temperature at which the reinforcing particulates were incorporated and the succeeding 20 °C testing temperature. It is vital to acknowledge that this study regards the preheated temperature of the mould as the designated testing temperature [55]. By substituting the G, k, b, ρ, ΔT, $\Delta\alpha$, V_r, and D values into Equations (4) and (5), the increase in MMCs' YS resulting from dislocation strengthening is found to be 63.01, 94.85, 112.03, and 138.61 MPa for the corresponding reinforcement contents of 0.5%, 1.0%, 1.5%, and 2.0% of nano-Al_2O_3 particles respectively, as presented in Figure 7a. The augmentation of micro-alumina reinforcement raises the dislocation density, hence inducing an enhancement in YS. Thermal strains at the interface of the nano-Al_2O_3 and matrix AA7150 during cooling from the processing temperature would be relieved by creating thermal mismatch dislocations around the Al_2O_3 nanoparticles. There would be adequate thermal stress surrounding the nanoparticles to initiate plastic deformation in the alloy matrix close to the interface area.

There is a noticeable disparity in the mechanical properties between the matrix and the dispersed particles inside particle-reinforced MMNCs. The observed gap gives rise to the formation of incoherent regions, resulting in a notable rise in dislocation density (ρ_{e+}, $m^{-1/2}$) at the interface between the matrix and the added particulates. In conjunction with incoherent regions, the heightened dislocation density amplifies precipitation mechanisms while also serving as a site for producing heterogeneous precipitation, as presented in Figure 7a [56]. The dissimilarity in the CTE between the matrix and reinforcing particulates, combined with thermal fluctuations during the fabrication of MMCs, can induce residual plastic strain in the AA7150 surrounding the Al_2O_3 particulates. This leads to the aforementioned strengthening effect through increased dislocation density (ρ_{e+}, $m^{-1/2}$). The strengthening effect due to dislocation density increases significantly with a decrease in nanoparticle size and an increase in the volume percentage, as shown in Figure 7b.

4.4. Grain-Refined Strengthening

The observed enhancement in strength can be ascribed to the improved fineness of the matrix grains. The impediment of the dislocation motion is caused by the heightened disorder in the lattice resulting from this refining. A lattice structure that is not properly aligned needs additional energy to alter the orientation of dislocation movement and to transition into neighboring grains. The area of the grain boundary increases owing to the grain refinement restricting the dislocation movement, aiding the improvement of the YS. The inclusion of nano-Al_2O_3 particulates at the grain boundaries of the matrix during the solidification impedes grain development, leading to a finer microstructure. Thus, it can be inferred from the findings of this research that there is a direct correlation between the level of limitation caused by an increased quantity of particulates and a reduction in the size of particulates to the nanoscale and the magnitude of the YS enhancement owing to the grain-structure refinement [57]. Estimating the enhancement in YS resulting from grain refining may be determined by employing the Hall–Petch relationship, as denoted by Equation (8):

$$\Delta\sigma_{Hall-Petch} = k\left(d^{-1/2} - d_0^{1/2}\right) \tag{8}$$

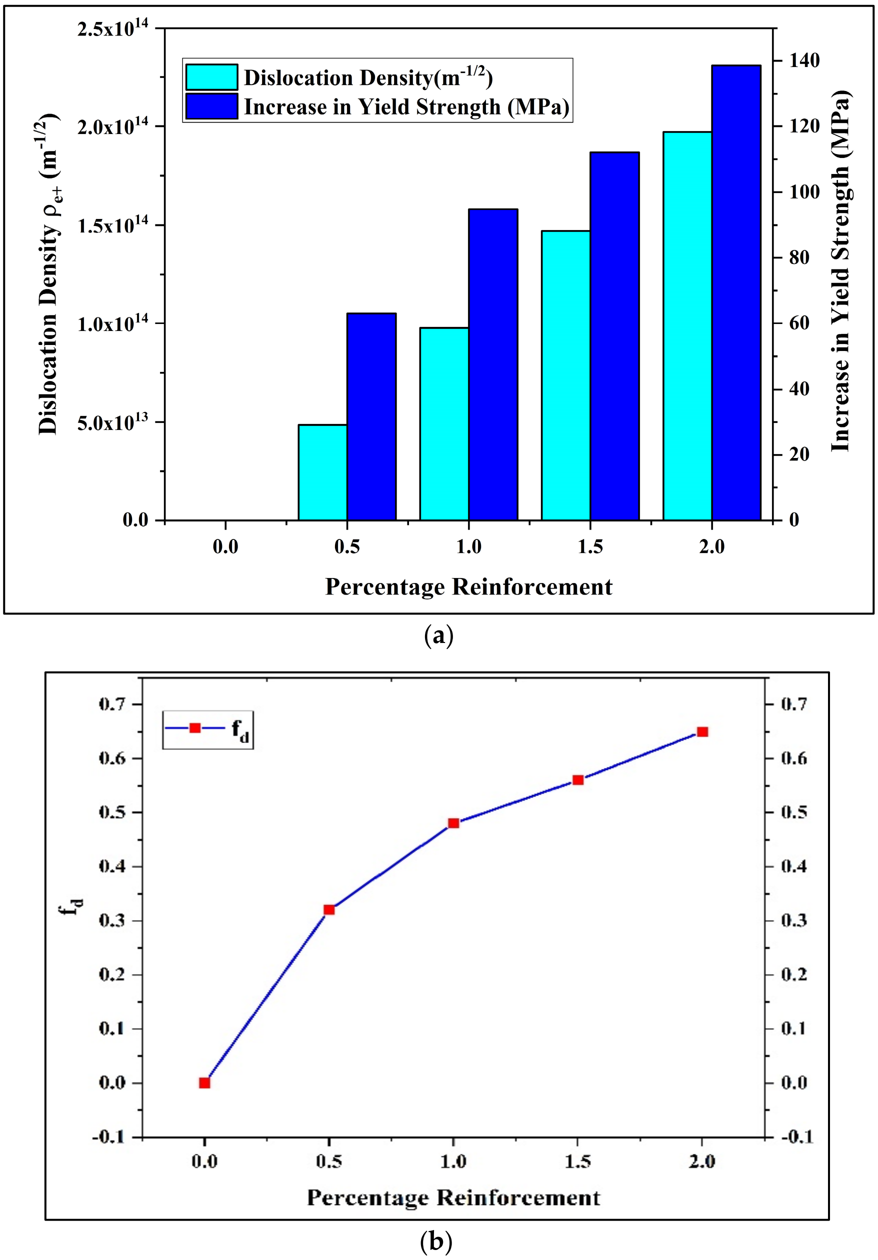

Figure 7. (**a**) Variation of dislocation density, increase in YS; and (**b**) f_d against percentage reinforcement in MMNCs.

Within this particular context, the variable "*k*" denotes the Hall–Petch slope pertaining to the matrix. The thermal conductivity value for pure Al is 74 × 10^{-3} MPa. The variables d and d_0 represent the matrix alloys and the reinforcing particle's average size, respectively. The average grain size values for different reinforcing circumstances were determined, and the distribution of these estimated grain sizes is depicted in Figure 8a–d. Consequently, the computed YS enhancement for the MMC resulting from the grain refinement strengthening effect is measured at 6.8, 7.7, 8.2, and 8.7 MPa for the respective reinforcement concentrations of 0.5, 1.0, 1.5, and 2.0% of nano-Al_2O_3 particulate reinforcement [58].

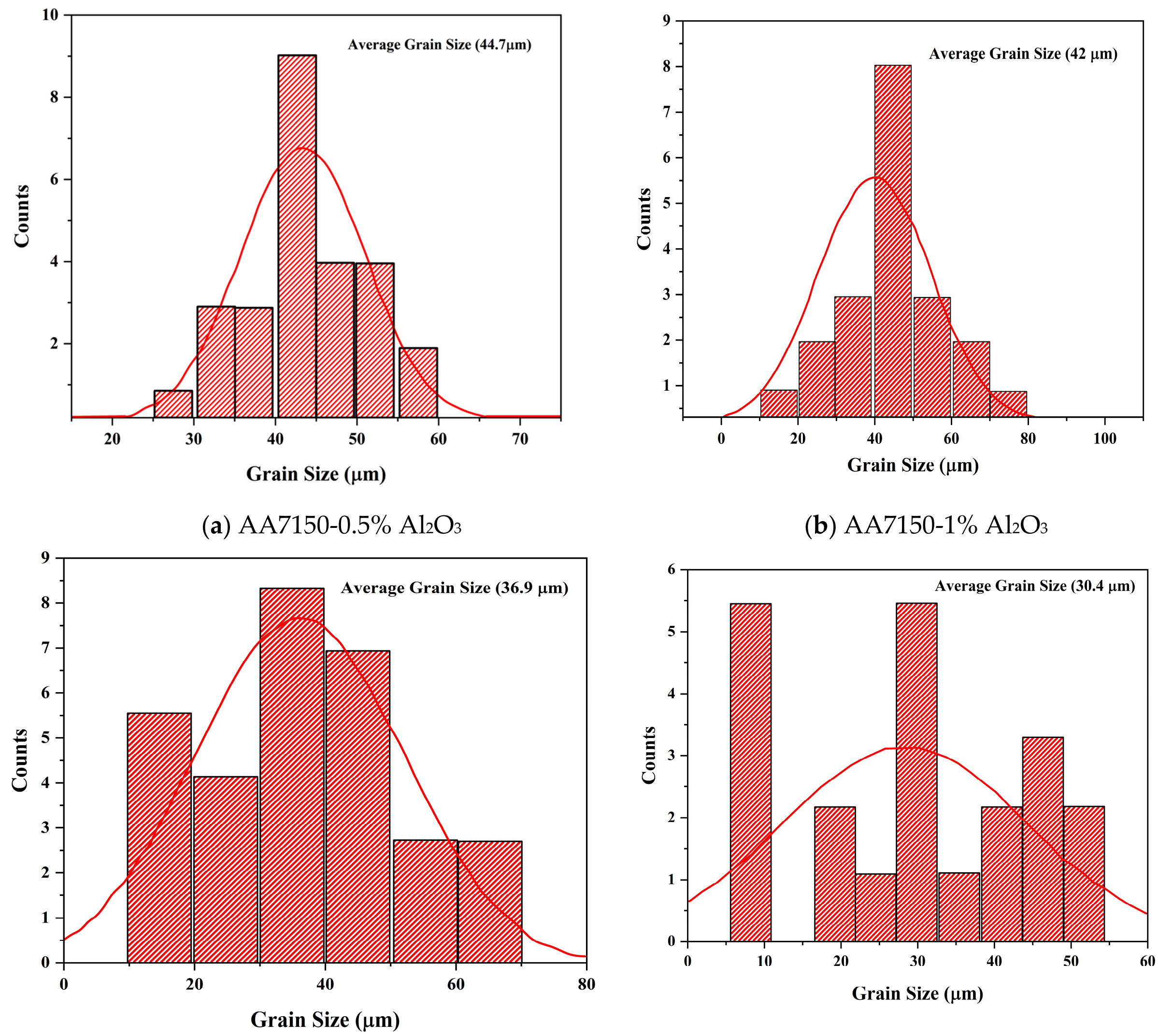

(**a**) AA7150-0.5% Al_2O_3 (**b**) AA7150-1% Al_2O_3

(**c**) AA7150-1.5% Al_2O_3 (**d**) AA7150-2% Al_2O_3

Figure 8. Grain-size distribution for AA7150-Al_2O_3 nanocomposites with: (**a**) 0.5; (**b**) 1.0; (**c**) 1.5; and (**d**) 2.0 wt.% reinforcement.

4.5. Prediction and Endorsement of Yield Strength

The investigation has successfully quantified each strengthening process's specific contributions to YS enhancement. The primary factor causing the rise in YS is the temperature mismatch, which was discovered to have the most substantial impact. This is followed by the strengthening effect known as Orowan strengthening. Nevertheless, the result of grain refinement on the increase in strength is somewhat limited, primarily attributed to the reduced Hall–Petch slope observed in pure Al [59]. The aforementioned results underscore the significance of thermal dislocation strengthening as the primary mechanism for enhancing the strength of nano-Al_2O_3-reinforced AA7150 matrix MMCs fabricated by the ultrasonic cavitation-supported stir-casting method. By integrating the impacts of various micromechanical strengthening processes that have been previously studied, Equation (9) was derived to estimate the enhanced YS of MMCs under distinct reinforcing circumstances [60]:

$$\sigma_{ym} = \sigma_{alloy} + \Delta\sigma_{Hall-Petch} + \sqrt{\left((\Delta\sigma_{Orowan})^2 + (\Delta\sigma_{CTE})^2\right)} \quad (9)$$

The symbol σ_{alloy} represents the AA7150 matrix yield strength in its as-cast form after undergoing ultrasonic cavitation treatment. The alloy yield strength (σ_{alloy}) was determined to be 114 MPa through experimental testing. Nevertheless, it was noted in Figure 8 that the experimentally determined YS values were lower than the values anticipated by theoretical calculations. The observed reduction in YS can be ascribed to the remainder of the clusters of nano-Al_2O_3 particles embedded inside the composite material. It is conceivable that, in contrast to the robustness of the relationship between ceramic particles and the matrix, the interparticle bond strength within these clusters exhibited a lesser degree of strength, giving rise to the formation of imperfections that eventually led to untimely structural deterioration [61].

4.6. Evaluation of Strengthening Mechanisms

A comparison was made between the experimentally observed YS values, and the composite yield strength was computed using load transfer strengthening and micromechanics processes. The findings indicate a tight alignment between the theoretically calculated values and the experimental data, with a negligible discrepancy of roughly 6–14%. The observed variance can be attributed to residual particles inside the composites and certain assumptions made during the theoretical computation.

Figure 9 illustrates the increase in YS for each given reinforcing situation, which may be attributable to several strengthening methods. Using Al_2O_3 nanoparticles as reinforcement substantially enhances the MMC's YS, emphasizing the significance of different strengthening techniques. The occurrence of particle agglomerates inside the composite material can result in the concentration of stress, which sequentially facilitates the crack's development and diminishes the efficacy of nanoparticle reinforcement. Consequently, this directly affects the composite's mechanical characteristics [62].

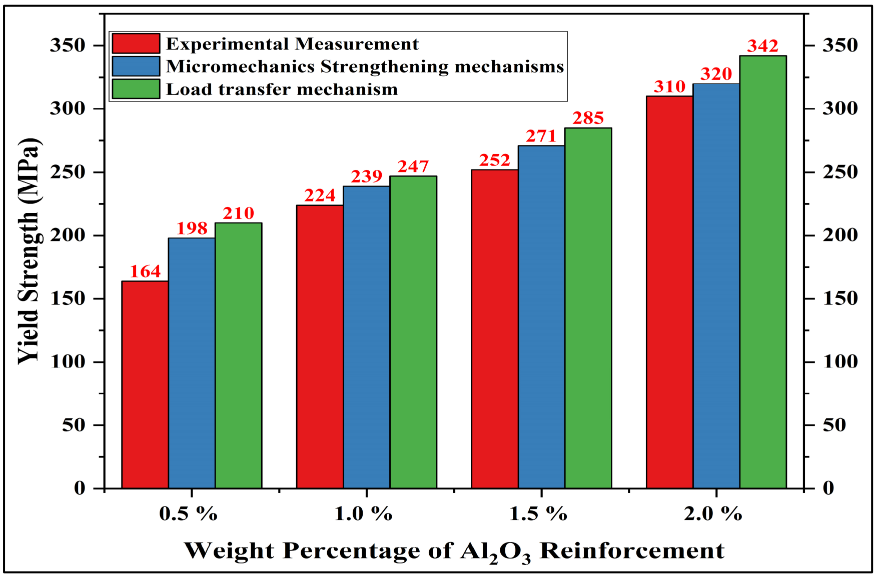

Figure 9. Experimental and theoretically predicted AA7150-Al_2O_3 nanocomposites' YS.

This study examined the micrographs displayed in Figure 3 and noted a progressive rise in the average particle cluster size from 1.083 to 3.505 μm when the wt.% of Al_2O_3 nanoparticles in the master alloy grew from 0.5% to 2.0%. It is crucial to acknowledge that as the particulate size shifts from the nanometer to the micrometer range, there are alterations in the extent to which reinforcement through the Orowan mechanism contributes to the load capacity [63].

The primary reinforcing mechanism in the produced AA7150-Al_2O_3 nanocomposites is thermal-imbalance-induced reinforcement. Orowan reinforcement, the Hall–Petch mechanism, and load transfer effects follow this. In addition, the amplifying effect resulting from variables such as the variation in CTE, interactions between dislocations in the matrix and particulate reinforcement, grain refinement, and the load transfer mechanism constantly exhibit an upward trend when the percentage of Al_2O_3 nanoparticles in the composite rises.

The enhancement in YS attained via grain refining is a synergistic outcome of using Al_2O_3 nanoparticles as a reinforcing agent and employing ultrasonic treatment. Nevertheless, the grain-refinement strengthening mechanism's impact on YS is insignificant when considering variations in the proportion of Al_2O_3 np. The primary influence on grain refinement is the pronounced effect of ultrasound-induced nucleation, as opposed to the grain refinement achieved by incorporating Al_2O_3 nanoparticles during the composites processing, as seen in Figure 10.

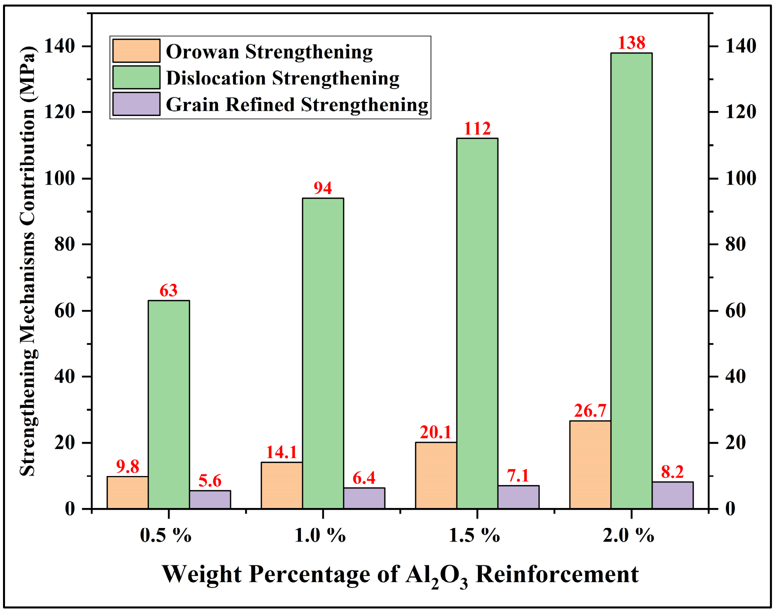

Figure 10. Strengthening mechanisms' effect on the YS of AA7150-Al_2O_3 nanocomposites.

Furthermore, the YS of MMNCs is enhanced by the interaction of many strengthening processes. Nevertheless, imperfections such as particle agglomerations and porosity, frequently observed in cast particulate-reinforced composites, unfavorably effect on YS. The discrepancies in the YS values for various percentages of nano-Al_2O_3 reinforcement can be attributed to these reasons [64].

4.7. Dry Sliding Wear Analyses of AA7150–Al_2O_3 MMNCs

The measurement of wear resistance in MMNCs was conducted by experimental analysis utilizing a pin-on-disc tribometer. Extensive studies have been undertaken on Al-MMNCs over the past 25 years to investigate their wear characteristics, resulting in the publication of various studies on this topic. The present investigation was conducted on a dry sliding wear experiment on the MMNCs under ambient conditions, adhering to the ASTM-G99 guidelines. The velocity of the sliding test sample was maintained at a 3.14 m/s, 6 km sliding distance, and a range of loads from 10 to 50 N. Figure 11a–e illustrates the specific wear rate noted at different sliding distances while subject to varied stresses. The results suggest a positive correlation between a specific wear rate and sliding distance. The observed phenomenon can be related to changes in frictional forces, increasing the temperature of the MMNCs. With an increase in temperature, the material experiences a decrease in hardness, leading to an escalation in wear.

The observation in Figure 11a indicated a progressive reduction in the specific wear rate as the reinforcement increased under a 10 N load, implying that an increase in hardness leads to enhanced wear resistance. According to the findings from Figure 11a, the composite materials consistently exhibited a lower specific wear rate than the matrix throughout all tested sliding distances. Furthermore, it was noted that the specific wear rate dropped as the Al_2O_3 concentration increased in the AA7150 matrix. The greater hardness of the MMNCs may be accredited to the improvements in material seizure and wear resistance [65].

The reinforced specimens exhibited a higher level of wear performance than the non-reinforced specimens. The observed decrease in the specific wear rate in the nano Al_2O_3 reinforced specimens can be attributed to the Orowan strengthening effect. This effect results in an enhancement of the hardness and strength of the samples and the generation of $MgZn_2$ precipitates. These precipitates hinder the movement of dislocations, thereby improving the ability of the composite samples to withstand the wear loads experienced during pin-on-disc wear tests. Another significant feature is the ability of the nano-Al_2O_3 particles to withstand the localized stresses that occur during dry slide wear testing. This ability protects the relatively soft outer surface of the AA7150 alloy matrix. The nano-Al_2O_3 reinforcement particles effectively hindered the direct contact between the softer matrix and the revolving steel disk on a significant scale [66]. With an increase in the load, the specific wear rate increases in non-reinforced specimens, and a reduction in the specific wear can be observed in the specimens with a higher wt.% of nanoparticle reinforcement, as shown in Figure 11b–e.

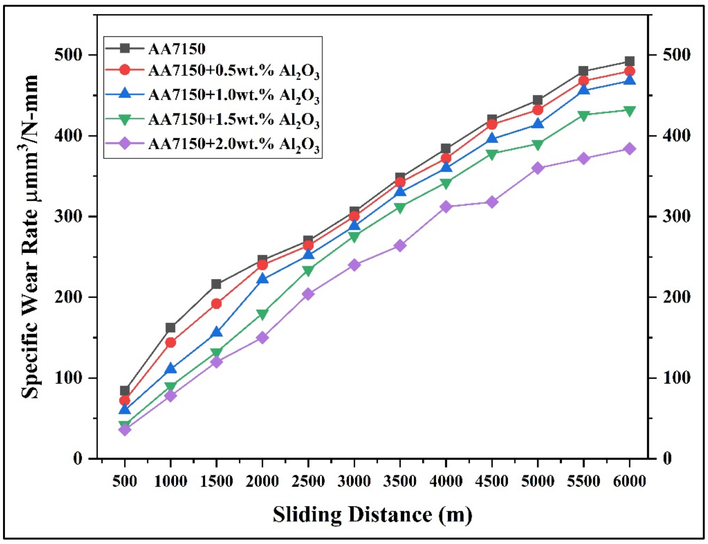

(**a**) The specific wear rate of MMNCs sliding at a load of 10 N.

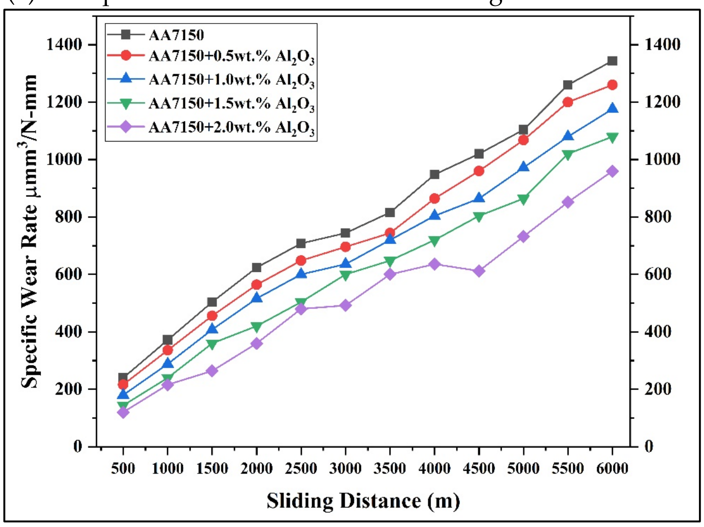

(**b**) The Specific Wear Rate of MMNCs sliding at 20 N load.

Figure 11. *Cont.*

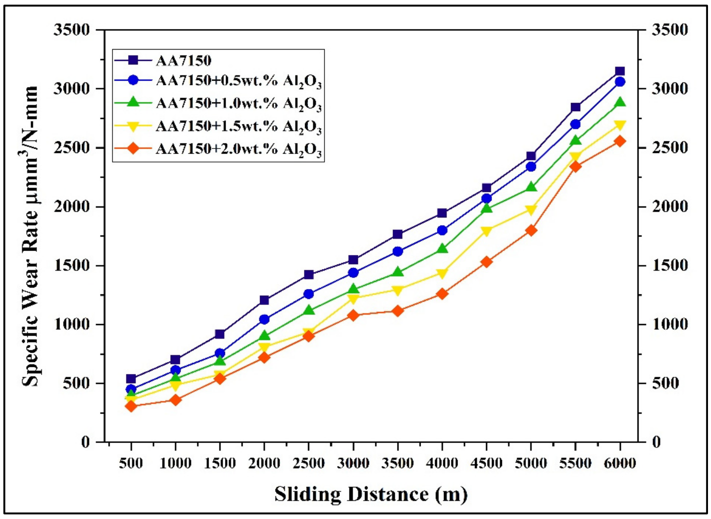

(**c**) The specific wear rate of MMNCs sliding at a load of 30 N.

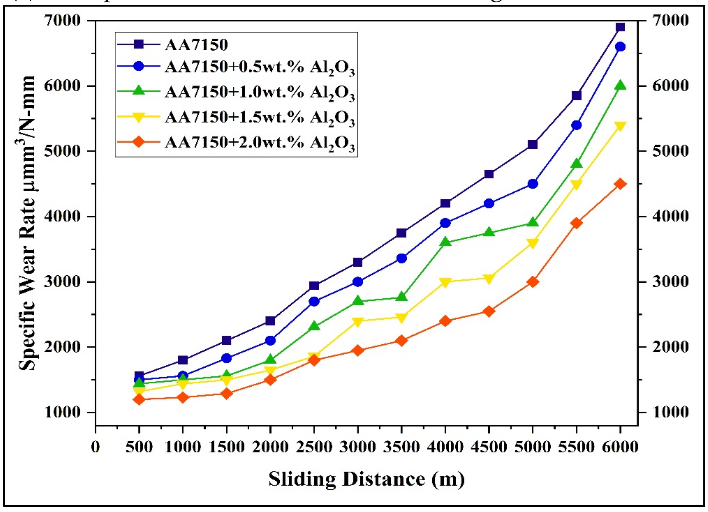

(**d**) The Specific Wear Rate of MMNCs sliding at a load of 40 N.

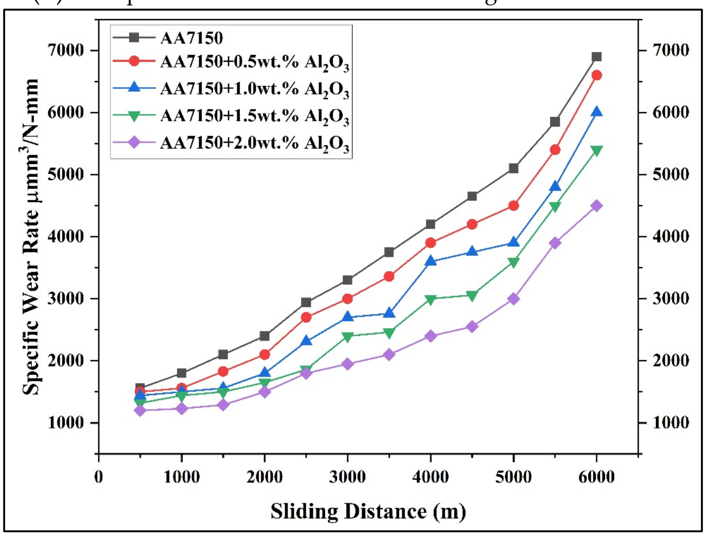

(**e**) The specific wear rate of MMNCs sliding at a load of 50 N.

Figure 11. (**a**–**e**) The specific wear rate of MMNCs with sliding distance at different loads.

Figure 12 depicts the relationship between load and specific wear rate, demonstrating their link. The wear rate of the AA7150 matrix and MMNCs is subject to the impact of the applied load, which is the predominant factor dictating wear behaviour. The sliding wear increases linearly in specimens with zero and up to 1.5 wt.% of Al_2O_3, at 2.0 wt.%, the variation is not linear, and due to the hardening of the specimen during sliding, the resistance against a specific wear rate is higher.

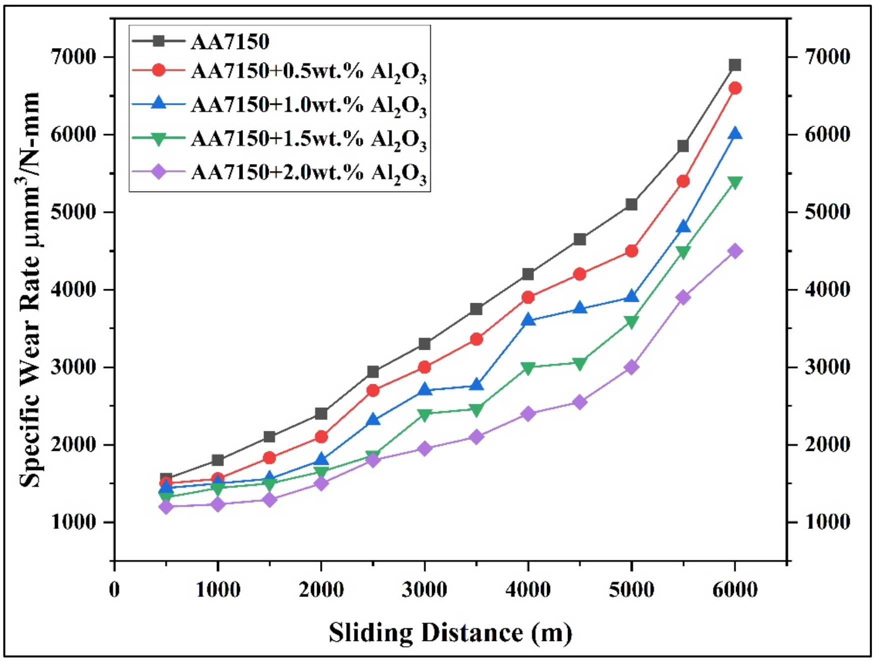

Figure 12. Effect of applied load on the specific wear rate with raise in the sliding distance of AA7150-2wt.% Al_2O_3 MMNCs.

The relationship between the wear rate and the applied load is linearly proportional, as per Archard's rule. Additionally, it is worth noting that composites exhibit a notably reduced wear rate. Furthermore, it has been shown that matrix materials and composites significantly increase specific wear rates by applying higher loads. Nevertheless, it is imperative to acknowledge that the resistance the composites show continuously exceeds that of the matrix, irrespective of the applied stress. Researchers have discovered that elevated loads are associated with delamination, leading to additional wear loss in the AA7150 matrix and composites [67].

The SEM analysis was employed to capture microphotographs of the worn-out surfaces of AA7150 and Al_2O_3 nanocomposites subjected to a 50 N load and 6 km sliding distance. The experimental readings indicated that the Al_2O_3 composites with a 2.0 wt.% component had reduced wear loss when subjected to a load of 50 N. The occurrence of grooves on the worn surfaces of the composite materials exhibited a decrease as the Al_2O concentration increased. The magnitude of grooves/tracks seen on the worn-out surface of the AA7150 and Al_2O_3 nanocomposites, including smaller volume percentage reinforcement, exhibited a notably increased significance at elevated loads, resulting in enhanced plastic deformation and severe wear. The discovery was discernible based on the SEM microphotographs depicted in Figure 13a–e. The utilization of SEM in morphological analyses revealed the existence of adhesive and abrasive wear processes in AA7150-Al_2O_3 MMNCs. Figure 13a illustrates severely damaged areas and deep abrasion grooves, which can be attributed to the low speed and delamination.

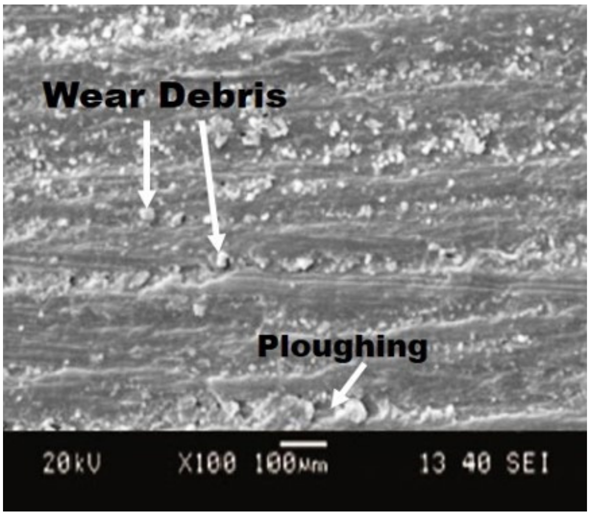

(**a**) Worn-out AA7150

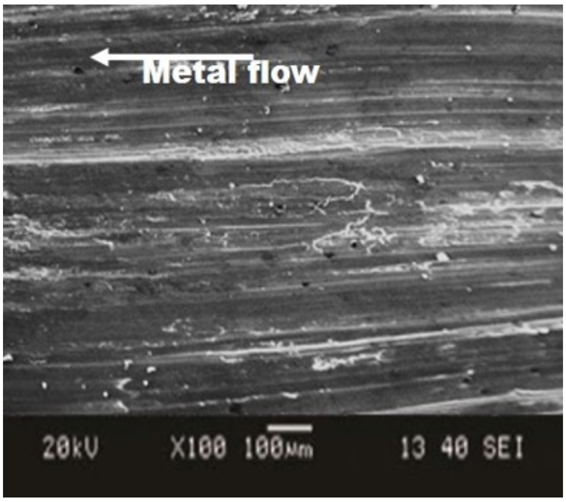

(**b**) Worn-out AA7150-0.5% Al_2O_3

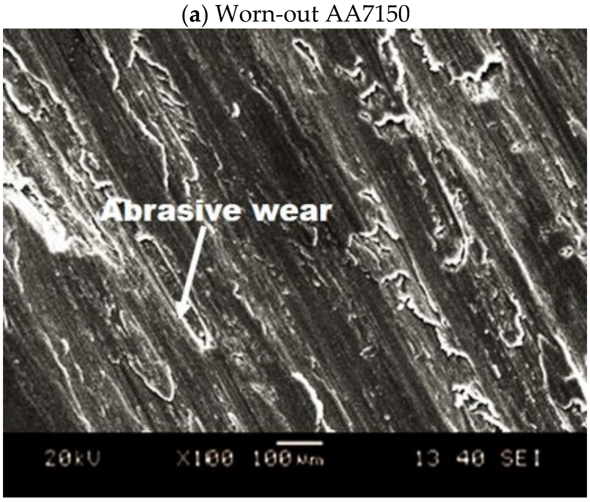

(**c**) worn-out AA7150-1% Al_2O_3

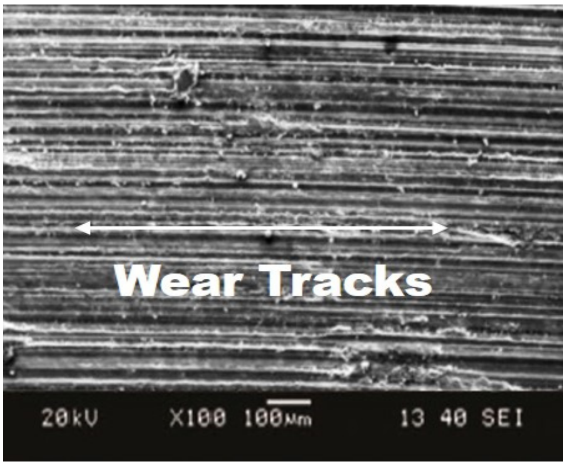

(**d**) Worn-out AA7150-1.5% Al_2O_3

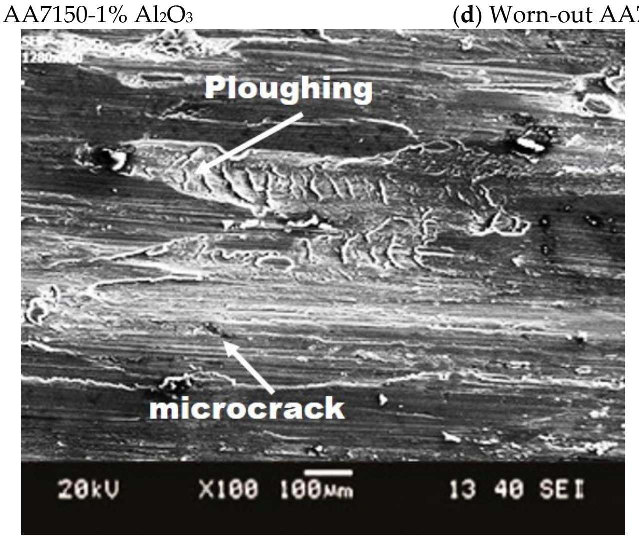

(**e**) AA7150-2% Al_2O_3

Figure 13. (**a**–**e**) SEM images of worn-out AA7150 alloy and Al715-0.5 to 2.0 wt.%. Al_2O_3 nanocomposites.

Additionally, the monolithic alloy exhibited signs of severe wear. The non-reinforced AA7150 alloy exhibits a notable deficiency in wear resistance, as seen by the substantial buildup of wear debris, the creation of craters, and the presence of ridges. Crater development may be attributed to delamination wear, the displacement of materials along the sliding path, and material shear on the sample's surface [68]. The ongoing sliding process led to the collection of wear debris, which resulted from the voids merging. The observed wear behavior may be attributed to the inferior hardness and load-bearing capability of the AA7150 alloy compared to its reinforced equivalent.

Similarly, it was observed that, with a rise in the Al_2O_3 filler content in the AA7150, there was a corresponding drop in wear loss, enhancing the material's wear resistance. The increased hardness of the AA7150-Al_2O_3 MMNCs can be attributed to this phenomenon. The material can experience an abrasive wear mechanism in the early phases of wear. With increased sliding distances, adherent particles may detach from the composite material. These detached particles can then act as abrasives between the composite pin and the counter disc, resulting in an abrasive wear mechanism. The SEM pictures in Figure 13a–e display worn-out surfaces, where the bright patches signify delaminated and worn-out particles caused by significant wear.

Additionally, the observed streaks in all MMNC samples are wear tracks that arise from steady-state wear, as mentioned in reference [69]. The occurrence of tiny fractures and cavity development during the pin-on-disc wear test decreases as the volume percentage of the reinforcement increases. The enhanced wear resistance seen in the AA7150 alloy composites supplemented with nano-Al_2O_3 particulates may be ascribed to the load-bearing capability of the nano-Al_2O_3 particles, which concurrently hinder the displacement of dislocations. Another factor contributing to the enhanced performance of composites reinforced with nano-Al_2O_3 is the minimal or near absence of agglomeration concerns, potentially resulting in the formation of porosity. The study using SEM Figure 13b–e identified the presence of adhesive and abrasive wear processes in the sample. The study's findings indicate that the samples' hardness and specific wear resistance were affected by incorporating different fractions and size distributions of Al_2O_3 particulates and by implementing efficient ultrasonic treatment. The incorporation of nano-Al_2O_3 into the Al7150 alloy matrix resulted in a decrease in the contact surface area and the uniform distribution of nano-reinforcement. Additionally, the adequate bonding between the nano-Al_2O_3 particles and the base matrix significantly improved the resistance to wear [70–72].

5. Conclusions

The significant conclusions in this current analysis are:

1. The optical microstructural study provides proof of the existence of nano-Al_2O_3 particles in all composites without any indication of oxide forms, secondary phases, or contaminants;
2. The use of ultrasonic vibrations was important in achieving uniform dispersion of nano-Al_2O_3 particles, establishing a desirable equilibrium between the malleability and robustness of the composites;
3. The composites that were created demonstrated a notable yield strength of 232 MPa, which was reached using just 2.0 wt.% of nano-Al_2O_3 particles. This resulted in a substantial increase of 97.52% in yield strength compared to the AA7150 matrix alloy treated with ultrasonics;
4. Theoretical estimations of the yield strength values of the AA7150-Al_2O_3 nanocomposites, utilizing micromechanics and load transfer strengthening processes, exhibit a strong correlation with the experimental findings;
5. According to theoretical expectations, the main factors that enhance mechanical strength in the AA7150-Al_2O_3 nanocomposites are a thermal mismatch, Orowan strengthening, the Hall–Petch mechanism, and load transfer effects;
6. The observed enhancements in mechanical strength can be credited to various strengthening mechanisms, including differences in the CTE, interactions between dislocations within the matrix and reinforcement particulates, grain refinement, and load transfer. Notably, these mechanisms consistently exhibited an increase in effectiveness as the percentage of Al_2O_3 nano contents in the composites was raised;

7. The resistance-to-wear of the MMNCs surpassed that of the underlying base alloy. The augmentation of applied loads and the extension of sliding lengths resulted in a proportional increase in the wear loss credited to wear;
8. Moreover, using Al_2O_3 as a reinforcing agent significantly enhanced the wear resistance of AA7150-Al_2O_3 MMNCs. The findings from extensive experiments suggest that incorporating a 2.0 wt.% of Al_2O_3 into AA7150 results in remarkable mechanical and tribological characteristics.

Author Contributions: Conceptualization, methodology, and investigation by K.C.M. and G.B.V.K.; data curation, writing—original draft preparation, writing—review and editing and visualization, R.P. All authors have read and agreed to the published version of the manuscript.

Funding: This research received no external funding.

Data Availability Statement: The data generated from the experiments conducted for this publication are available upon request. The authors are committed to promoting transparency and reproducibility in research. Interested parties may contact G B Veeresh Kumar at veereshkumargb@nitandhra.ac.in, to request access to the dataset. The authors will make every effort to provide the data promptly, ensuring that it aligns with ethical and legal considerations. By sharing our data, we aim to facilitate collaboration and further exploration of the findings presented in this manuscript.

Acknowledgments: The authors acknowledge and express gratitude for the continuous support provided by the administration of the National Institute of Technology, Andhra Pradesh, Tadepalligudem, and Amrita Vishwa Vidyapeetham, Bengaluru campus, and CMR Engineering College, Medchal Road, Hyderabad Telangana, for their consistent inspiration and encouragement throughout the research work.

Conflicts of Interest: The authors declare no conflicts of interest. The research work has no external funders, and no financial institution had any role in the design of the study, in the collection, analyses, or interpretation of data, in the writing of the manuscript, or in the decision to publish the results.

References

1. Rawal, S.P. Metal-matrix composites for space applications. *JOM* **2001**, *53*, 14–17. [CrossRef]
2. Pandey, A.K.; Chatterjee, S.; Mahapatra, S.S. Analysis and characterization of weld quality during butt welding through friction stir welding. *Indian J. Eng. Mater. Sci.* **2019**, *26*, 298–310.
3. Williams, J.C.; Starke, E.A., Jr. Progress in structural materials for aerospace systems. *Acta Mater.* **2003**, *51*, 5775–5799. [CrossRef]
4. Zhan, Y.; Zhang, G. Graphite and SiC hybrid particles reinforced copper composite and its tribological characteristic. *J. Mater. Sci. Lett.* **2003**, *22*, 1087–1089. [CrossRef]
5. Salem, H.; El-Eskandarany, S.H.; Kandil, A.; Fattah, H.A. Bulk behaviour of ball-milled AA2124 nanostructured powders reinforced with TiC. *J. Nanomater.* **2009**, *2009*, 479185. [CrossRef]
6. Sahu, A.K.; Mahapatra, S.S.; Chatterjee, S. Optimization of Electrical Discharge Coating Process Using MOORA Based Firefly Algorithm. In Proceedings of the ASME 2017 Gas Turbine India Conference, Bangalore, India, 7–8 December 2017; p. V002T10A005, ASME.
7. Cholkar, A.; McCann, R.; Perumal, G.; Chatterjee, S.; Swayne, M.; Kinahan, D.; Brabazon, D. Advances in laser-based surface texturing for developing antifouling surfaces: A comprehensive review. *Appl. Surf. Sci. Adv.* **2023**, *18*, 100513. [CrossRef]
8. Kumar, G.B.V.; Chowdary, G.V.; Vamsi, M.S.; Reddy, K.J.; Nagaral, M.; Naresh, K. Effects of addition of Titanium Diboride and Graphite Particulate Reinforcements on Physical, Mechanical and Tribological properties of Al6061 Alloy based Hybrid Metal Matrix Composites. *Adv. Mater. Process. Technol.* **2021**, *8*, 2259–2276. [CrossRef]
9. Kumar, G.; Panigrahy, P.P.; Nithika, S.; Pramod, R.; Rao, C. Assessment of mechanical and tribological characteristics of Silicon Nitride reinforced aluminum metal matrix composites. *Compos. Part B Eng.* **2019**, *175*, 107138. [CrossRef]
10. Khakbiz, M.; Akhlaghi, F. Synthesis and structural characterization of Al–B4C nano-composite powders by mechanical alloying. *J. Alloys Compd.* **2009**, *479*, 334–341. [CrossRef]
11. Kumar, G.; Pramod, R.; Sekhar, C.G.; Bhanumurthy, T. Investigation of physical, mechanical and tribological properties of Al6061–ZrO2 nano-composites. *Heliyon* **2019**, *5*, e02858. [CrossRef]
12. Sajjadi, S.; Parizi, M.T.; Ezatpour, H.; Sedghi, A. Fabrication of A356 composite reinforced with micro and nano Al2O3 particles by a developed compocasting method and study of its properties. *J. Alloys Compd.* **2012**, *511*, 226–231. [CrossRef]
13. Cao, G.; Konishi, H.; Li, X. Mechanical properties and microstructure of Mg/SiC nanocomposites fabricated by Ultrasonic cav-itation based nano-manufacturing. *J. Manuf. Sci. Eng.* **2008**, *130*, 031105. [CrossRef]
14. Krishnan, P.K.; Arunachalam, R.; Husain, A.; Al-Maharbi, M. Studies on the Influence of Stirrer Blade Design on the Microstructure and Mechanical Properties of a Novel Aluminum Metal Matrix Composite. *J. Manuf. Sci. Eng.* **2020**, *143*, 021008. [CrossRef]

15. Lü, S.; Xiao, P.; Yuan, D.; Hu, K.; Wu, S. Preparation of Al matrix nanocomposites by diluting the composite granules containing nano-SiCp under ultrasonic vibration. *J. Mater. Sci. Technol.* **2018**, *34*, 1609–1617. [CrossRef]
16. Wu, J.; Zhou, S.; Li, X. Ultrasonic Attenuation Based Inspection Method for Scale-up Production of A206–Al2O3 Metal Matrix Nanocomposites. *J. Manuf. Sci. Eng.* **2015**, *137*, 011013. [CrossRef]
17. Yuan, D.; Hu, K.; Lü, S.; Wu, S.; Gao, Q. Preparation and properties of nano-SiC_p/A356 composites synthesised with a new process. *Mater. Sci. Technol.* **2018**, *34*, 1415–1424. [CrossRef]
18. Pu, B.; Lin, X.; Li, B.; Chen, X.; He, C.; Zhao, N. Effect of SiC nanoparticles on the precipitation behavior and mechanical properties of 7075Al alloy. *J. Mater. Sci.* **2020**, *55*, 6145–6160. [CrossRef]
19. Poovazhagan, L.; Kalaichelvan, K.; Rajadurai, A. Preparation of SiC Nanoparticulates Reinforced Aluminum Matrix Nanocomposites by High Intensity Ultrasonic Cavitation Process. *Trans. Indian Inst. Met.* **2013**, *67*, 229–237. [CrossRef]
20. Yuan, D.; Yang, X.; Wu, S.; Lü, S.; Hu, K. Development of high strength and toughness nano-SiCp/A356 composites with ultrasonic vibration and squeeze casting. *J. Mater. Process. Technol.* **2019**, *269*, 1–9. [CrossRef]
21. Hauschwitz, P.; Jagdheesh, R.; Rostohar, D.; Brajer, J.; Kopeček, J.; Jiřícek, P.; Houdková, J.; Mocek, T. Hydrophilic to ultrahydrophobic transition of Al 7075 by affordable ns fiber laser and vacuum processing. *Appl. Surf. Sci.* **2020**, *505*, 144523. [CrossRef]
22. Manikandan, R.; Arjunan, T.; Akhil, R.; Nath, O.P. Studies on micro structural characteristics, mechanical and tribological behaviours of boron carbide and cow dung ash reinforced aluminium (Al 7075) hybrid metal matrix composite. *Compos. Part B Eng.* **2020**, *183*, 107668. [CrossRef]
23. Yang, Y.; Lan, J.; Li, X. Study on bulk aluminum matrix nano-composite fabricated by ultrasonic dispersion of nano-sized SiC particles in molten aluminum alloy. *Mater. Sci. Eng. A* **2004**, *380*, 378–383. [CrossRef]
24. Hashim, J.; Looney, L.; Hashmi, M. The enhancement of wettability of SiC particles in cast aluminium matrix composites. *J. Am. Acad. Dermatol.* **2001**, *119*, 329–335. [CrossRef]
25. Su, H.; Gao, W.; Zhang, H.; Liu, H.; Lu, J.; Lu, Z. Optimization of Stirring Parameters through Numerical Simulation for the Preparation of Aluminum Matrix Composite by Stir Casting Process. *J. Manuf. Sci. Eng.* **2010**, *132*, 061007. [CrossRef]
26. Gao, Q.; Wu, S.; Lü, S.; Xiong, X.; Du, R.; An, P. Improvement of particles distribution of in-situ 5 vol% TiB2 particulates reinforced Al-4.5Cu alloy matrix composites with ultrasonic vibration treatment. *J. Alloys Compd.* **2017**, *692*, 1–9. [CrossRef]
27. Xu, H.; Jian, X.; Meek, T.T.; Han, Q. Degassing of molten aluminum A356 alloy using ultrasonic vibration. *Mater. Lett.* **2004**, *58*, 3669–3673. [CrossRef]
28. Tsunekawa, Y.; Suzuki, H.; Genma, Y. Application of ultrasonic vibration to in situ MMC process by electromagnetic melt stirring. *Mater. Des.* **2001**, *22*, 467–472. [CrossRef]
29. Kumar, N.; Gautam, G.; Gautam, R.K.; Mohan, A.; Mohan, S. A Study on Mechanical Properties and Strengthening Mechanisms of AA5052/ZrB2 In Situ Composites. *J. Eng. Mater. Technol.* **2017**, *139*, 011002. [CrossRef]
30. Chen, L.-Y.; Peng, J.-Y.; Xu, J.-Q.; Choi, H.; Li, X.-C. Achieving uniform distribution and dispersion of a high percentage of nanoparticles in metal matrix nanocomposites by solidification processing. *Scr. Mater.* **2013**, *69*, 634–637. [CrossRef]
31. Kumar, G.B.V.; Reddy, D.G.; Reddy, C.V.; Sriteja, C.; Pramod, R. Investigation of Mechanical and Tribological Properties of Al6061–TiB2 Metal Matrix Composites. *Mater. Perform. Charact.* **2020**, *9*, 139–150. [CrossRef]
32. Sathishkumar, P.; Deepakaravind, V.; Gopal, P.; Azhagiri, P. Analysis the mechanical properties and material characterization on Magnesium Metal Matrix Nano composites through stir casting process. *Mater. Today Proc.* **2021**, *46 Pt 17*, 7436–7441. [CrossRef]
33. Kumar, G.B.V.; Pramod, R.; Gouda, P.S.S.; Rao, C.S.P. Effect of Tungsten Carbide Reinforcement on the Aluminum 6061 Alloy. *J. Test. Eval.* **2018**, *47*, 2613–2629. [CrossRef]
34. Chawla, N.; Williams, J.; Saha, R. Mechanical behavior and microstructure characterization of sinter-forged SiC particle reinforced aluminum matrix composites. *J. Light Met.* **2002**, *2*, 215–227. [CrossRef]
35. Soni, S.K.; Manimaran, D.; Thomas, S.B.; Thomas, B. Microstructure and mechanical characterization of Al6061 based composite and nanocomposites prepared via conventional and ultrasonic-assisted melt-stirring techniques. *Mater. Today Commun.* **2023**, *34*, 105222. [CrossRef]
36. Nie, K.; Wang, X.; Wu, K.; Hu, X.; Zheng, M. Development of SiCp/AZ91 magnesium matrix nanocomposites using ultrasonic vibration. *Mater. Sci. Eng. A* **2012**, *540*, 123–129. [CrossRef]
37. Yang, H.; Jiang, L.; Balog, M.; Krizik, P.; Schoenung, J.M. Reinforcement Size Dependence of Load Bearing Capacity in Ultrafine-Grained Metal Matrix Composites. *Met. Mater. Trans. A* **2017**, *48*, 4385–4392. [CrossRef]
38. Li, S.; Yue, X.; Li, Q.; Peng, H.; Dong, B.; Liu, T.; Yang, H.; Fan, J.; Shu, S.; Qiu, F.; et al. Development and applications of aluminum alloys for aerospace industry. *J. Mater. Res. Technol.* **2023**, *27*, 944–983. [CrossRef]
39. Sha, J.; Lv, Z.; Lin, G.; Dai, J.; Zu, Y.; Xian, Y.; Zhang, W.; Cui, D.; Yan, C. Synergistic strengthening of aluminum matrix composites reinforced by SiC nanoparticles and carbon fibers. *Mater. Lett.* **2019**, *262*, 127024. [CrossRef]
40. Mousavian, R.T.; Behnamfard, S.; Khosroshahi, R.A.; Zavašnik, J.; Ghosh, P.; Krishnamurthy, S.; Heidarzadeh, A.; Brabazon, D. Strength-ductility trade-off via SiC nanoparticle dispersion in A356 aluminium matrix. *Mater. Sci. Eng. A* **2020**, *771*, 138639. [CrossRef]
41. Zhao, L.; Lu, H.; Gao, Z. Microstructure and Mechanical Properties of Al/Graphene Composite Produced by High-Pressure Torsion. *Adv. Eng. Mater.* **2015**, *17*, 976–981. [CrossRef]

42. Hassan, S.; Gupta, M. Effect of particulate size of Al2O3 reinforcement on microstructure and mechanical behavior of solidification processed elemental Mg. *J. Alloys Compd.* **2006**, *419*, 84–90. [CrossRef]
43. Zhang, Z.; Chen, D.L. Contribution of Orowan strengthening effect in particulate-reinforced metal matrix nanocomposites. *Mater. Sci. Eng. A* **2008**, *483*, 148–152. [CrossRef]
44. Nampoothiri, J.; Balasundar, I.; Raghu, T.; Ravi, K.R. Structural and Mechanical Behavior of Al-4.4Cu/2TiB2In-Situ Nanocomposites Fabricated by Post-In-Situ Reaction Ultrasonic Processing. *Met. Mater. Trans. B* **2020**, *51*, 149–160. [CrossRef]
45. Gupta, R.; Chaudhari, G.; Daniel, B. Strengthening mechanisms in ultrasonically processed aluminium matrix composite with in-situ Al3Ti by salt addition. *Compos. Part B Eng.* **2017**, *140*, 27–34. [CrossRef]
46. Jayalakshmi, S.; Gupta, S.; Sankaranarayanan, S.; Sahu, S.; Gupta, M. Structural and mechanical properties of Ni60Nb40 amorphous alloy particle reinforced Al-based composites produced by microwave-assisted rapid sintering. *Mater. Sci. Eng. A* **2013**, *581*, 119–127. [CrossRef]
47. Zhang, Q.; Xiao, B.; Wang, W.; Ma, Z. Reactive mechanism and mechanical properties of in situ composites fabricated from an Al–TiO2 system by friction stir processing. *Acta Mater.* **2012**, *60*, 7090–7103. [CrossRef]
48. Wang, M.; Chen, D.; Chen, Z.; Wu, Y.; Wang, F.; Ma, N.; Wang, H. Mechanical properties of in-situ TiB2/A356 composites. *Mater. Sci. Eng. A* **2014**, *590*, 246–254. [CrossRef]
49. Chen, F.; Chen, Z.; Mao, F.; Wang, T.; Cao, Z. TiB2 reinforced aluminum based in situ composites fabricated by stir casting. *Mater. Sci. Eng. A* **2015**, *625*, 357–368. [CrossRef]
50. Saba, F.; Zhang, F.; Liu, S.; Liu, T. Reinforcement size dependence of mechanical properties and strengthening mechanisms in diamond reinforced titanium metal matrix composites. *Compos. Part B Eng.* **2018**, *167*, 7–19. [CrossRef]
51. Jiang, M.; Zhang, X.; Mei, H.; Xu, S.; Liu, L. The coupled effects of grain boundary strengthening and Orowan strengthening examined by dislocation dynamics simulations. *Comput. Mater. Sci.* **2024**, *231*, 112602. [CrossRef]
52. Xuan, Y.; Nastac, L. The role of ultrasonic cavitation in refining the microstructure of aluminum based nanocomposites during the solidification process. *Ultrasonics* **2018**, *83*, 94–102. [CrossRef]
53. Kumar, G.B.V.; Gouda, P.S.S.; Pramod, R.; Chowdary, U.S.K.; Subash, T.; Vamsi, M.S.; Naresh, K. Development and experimental evaluation of titanium diboride particulate reinforcements on the Al6061 alloy composites properties. *Adv. Mater. Process. Technol.* **2020**, *8*, 1209–1225. [CrossRef]
54. Madhukar, P.; Selvaraj, N.; Kumar, G.V.; Rao, C.; Mohammad, F.; Chavali, M. Effect of TiCnp on microstructure and mechanical behaviour of high-performance Al7150-TiC nanocomposites. *Mater. Sci. Eng. B* **2021**, *265*, 115034. [CrossRef]
55. Shen, G.; Chen, X.; Yan, J.; Fan, L.; Yang, Z.; Zhang, J.; Guan, R. Effects of heat treatment processes on the mechanical properties, microstructure evolution, and strengthening mechanisms of Al–Mg–Zn–Cu alloy. *J. Mater. Res. Technol.* **2023**, *27*, 5380–5388. [CrossRef]
56. Dey, D.; Bhowmik, A.; Biswas, A. Characterization of physical and mechanical properties of aluminium based composites reinforced with titanium diboride particulates. *J. Compos. Mater.* **2021**, *55*, 1979–1991. [CrossRef]
57. Gautam, G.; Kumar, N.; Mohan, A.; Gautam, R.; Mohan, S. Strengthening mechanisms of (Al_3Zr_{mp} + ZrB_{2np})/AA5052 hybrid composites. *J. Compos. Mater.* **2016**, *50*, 4123–4133. [CrossRef]
58. Manjunath, R.; Kumar, D.; Kumar, A. A Review on the Significance of Hybrid Particulate Reinforcements on the Mechanical and Tribological Properties of Stir-Casted Aluminum Metal Matrix Composites. *J. Bio Tribo Corros.* **2021**, *7*, 122. [CrossRef]
59. Reddy, A.P.; Krishna, P.V.; Rao, R.N. Tribological Behaviour of Al6061–2SiC-xGr Hybrid Metal Matrix Nanocomposites Fabricated through Ultrasonically Assisted Stir Casting Technique. *Silicon* **2019**, *11*, 2853–2871. [CrossRef]
60. Mazahery, A.; Ostadshabani, M. Investigation on mechanical properties of nano-Al_2O_3-reinforced aluminum matrix composites. *J. Compos. Mater.* **2011**, *45*, 2579–2586. [CrossRef]
61. Madhukar, P.; Mishra, V.; Selvaraj, N.; Rao, C.S.P.; Basavaraja, V.K.G.; Seetharam, R.; Chavali, M.; Mohammad, F.; Soleiman, A.A. Influence of Ultrasonic Vibration towards the Microstructure Refinement and Particulate Distribution of AA7150-B4C Nanocomposites. *Coatings* **2022**, *12*, 365. [CrossRef]
62. Bhowmik, A.; Kumar, R.; Babbar, A.; Romanovski, V.; Roy, S.; Patnaik, L.; Kumar, J.P.; Alawadi, A.H. Analysis of physical, mechanical and tribological behavior of Al7075-fly ash composite for lightweight applications. *Int. J. Interact. Des. Manuf. IJIDeM* **2023**, 1–14. [CrossRef]
63. Ma, P.; Jia, Y.; Gokuldoss, P.K.; Yu, Z.; Yang, S.; Zhao, J.; Li, C. Effect of Al_2O_3 Nanoparticles as Reinforcement on the Tensile Behavior of Al-12Si Composites. *Metals* **2017**, *7*, 359. [CrossRef]
64. Akbari, M.K.; Baharvandi, H.; Mirzaee, O. Fabrication of nano-sized Al2O3 reinforced casting aluminum composite focusing on preparation process of reinforcement powders and evaluation of its properties. *Compos. Part B Eng.* **2013**, *55*, 426–432. [CrossRef]
65. Jayakumar, V.; Bharathiraja, G.; Palani, K. Investigations on mechanical and wear behaviour of graphene and zirconia reinforced AA6061 hybrid nanocomposites using ANN and Sugeno-type fuzzy inference systems. *Mater. Res. Express* **2022**, *9*, 115002. [CrossRef]
66. Kareem, A.; Abu Qudeiri, J.; Abdudeen, A.; Ahammed, T.; Ziout, A. A Review on AA 6061 Metal Matrix Composites Produced by Stir Casting. *Materials* **2021**, *14*, 175. [CrossRef] [PubMed]
67. Uday, K.N.; Rajamurugan, G. Effect of stir casting parameters and mono/hybrid reinforcements on aluminium metal matrix composite—A review. *Proc. Inst. Mech. Eng. Part C J. Mech. Eng. Sci.* **2022**, *236*, 4904–4920. [CrossRef]
68. Mondal, S. Aluminum or Its Alloy Matrix Hybrid Nanocomposites. *Met. Mater. Int.* **2021**, *27*, 1–17. [CrossRef]

69. Mohanavel, V.; Prasath, S.; Yoganandam, K.; Tesemma, B.G.; Kumar, S.S. Optimization of wear parameters of aluminium composites (AA7150/10 wt%WC) employing Taguchi approach. *Mater. Today Proc.* **2020**, *33*, 4742–4745. [CrossRef]
70. Rahman, M.A.; Sirajudeen, N.; Karunanithi, R. Hardness and dry sliding wear behavior of SiC reinforced Al 7150 alloy composite synthesized under the influence of aging, varying compaction pressures, particle size and volume fraction of ceramic particulates by hot compaction technique. *Mater. Res. Express* **2019**, *6*, 066536. [CrossRef]
71. Rahman, A.; Haque, S. The Influence of Heat Treatment and High Energy Ball Milling on the Density, Hardness, and Wear Behavior of Al 7150 Alloy via Hot Uniaxial Compaction. *Iran. J. Mater. Sci. Eng. IJMSE* **2022**, *19*, 100–112.
72. Madhukar, P.; Selvaraj, N.; Rao, C.; Kumar, G.V. Fabrication and characterization two step stir casting with ultrasonic assisted novel AA7150-hBN nanocomposites. *J. Alloys Compd.* **2020**, *815*, 152464. [CrossRef]